Exosomal miR-218-5p/miR-363-3p from Endothelial Progenitor Cells Ameliorate Myocardial Infarction by Targeting the P53/JMY Signaling Pathway

Xiao Ke
Fuwai Hospital, Chinese Academy of Medical Science
Rongfeng Yang
The Eighth Affiliated Hospital, Sun Yat-sen Univer
Fang Wu
The First Affiliated Hospital of Sun Yat-sen Unive
Xing Wang
The First Affiliated Hospital of Sun Yat-sen Unive
Jiawen Liang
The First Affiliated Hospital of Sun Yat-sen Unive
Xun Hu
The First Affiliated Hospital of Sun Yat-sen Unive
Chengheng Hu (huchengh@mail.sysu.edu.cn)
The First Affiliated Hospital of Sun Yat-sen University https://orcid.org/0000-0003-4243-0618

Research

Keywords: exosomes, myocardial fibrosis, myocardial infarction, microRNA, endothelial progenitor cells, P53/JMY

Posted Date: January 18th, 2021

DOI: https://doi.org/10.21203/rs.3.rs-146749/v1

Abstract

Background

Accumulating evidence has shown that endothelial progenitor cell-derived exosomes (EPC-Exos) can ameliorate myocardial fibrosis. The purpose of the present study was to investigate the effects of EPC-Exos-derived microRNAs (miRNAs) on myocardial infarction (MI).

Methods

A miRNA-Seq dataset of miRNAs differentially expressed between EPCs and exosomes was collected. Quantitative real-time polymerase chain reaction (qRT-PCR) was used to validate the miRNA expression indicated by miRNA-Seq. Immunofluorescence, cell proliferation and angiogenesis assays were employed to investigate the effects of miRNAs on cardiac fibroblasts (CFs) *in vitro*. Interactions between miRNAs and their respective targets were examined via immunoblotting, qRT-PCR and luciferase reporter assays. An MI rat model was constructed, and various staining and immunohistochemical assays were performed to explore the mechanisms underlying the miRNA-mediated effects on MI.

Results

miR-363-3p and miR-218-5p were enriched in EPC-Exos, and miR-218-5p and miR-363-3p mimic or inhibitor enhanced or suppressed CF proliferation and angiogenesis, respectively. miR-218-5p and miR-363-3p regulated P53 and junction-mediating and regulatory protein (JMY) by binding to the promoter region of P53 and the 3’ untranslated region of JMY. Additionally, treatment of CFs with exo-miR-218-5p or miR-363-3p mimic upregulated P53 and down-regulated JMY expression, promoted mesenchymal-endothelial transition and inhibited myocardial fibrosis. Administration of exosomes containing miR-218-5p mimic or miR-363-3p mimic ameliorated left coronary artery ligation-induced MI and restored myocardial tissue integrity in the MI model rats.

Conclusions

In summary, these results show that the protective ability of EPC-Exos against MI was mediated by the shuttled miR-218-5p or miR-363-3p via targeting of the P53/JMY signaling pathway.

Background

Cardiovascular diseases account for over 40% of deaths annually and are the leading cause of death around the world [1]. Of note, chronic heart failure (CHF) is the leading cause of cardiovascular mortality, with an increased prevalence in recent years [2]. Myocardial infarction (MI)-induced remodeling of the left ventricle (LV) is the most common cause of CHF [3]. The clinical features of MI include LV dilatation, cardiomyocyte death and myocardial remodeling [3, 4]. Irreversible cardiac tissue damage caused by MI leads to myocardial fibrosis (MF), ventricular remodeling, cardiac dysfunction [5] and finally heart failure [6–8]. MF is the final pathological consequence of cardiovascular disease and is characterized by

abnormal thickening of heart valves or excessive deposition of extracellular matrix in the cardiac muscle [9], which results in progression to heart failure [10, 11]. Therefore, alleviation or prevention of MF is an important therapeutic strategy for management of MI.

Endothelial progenitor cells (EPCs) originate from the bone marrow, localize within damaged tissues and play a vital role in regeneration of the endothelial lining of damaged blood vessels during heart attacks [12], representing a possible therapeutic treatment for MI. Previous studies have reported that a higher level of circulating EPCs predicted a better outcome for patients with cardiovascular disease [13]. Small-scale clinical trials have confirmed EPCs as a potential treatment for MF [14] and MI [15, 16]. However, to date, the functional substrates and potential molecular mechanisms associated with EPC therapy for MF or MI have not been thoroughly elucidated.

Exosomes are secreted by various cell types [17, 18] and contain various paracrine factors, including proteins, lipids and RNA. Moreover, exosomes vary in diameter from 40 to 100 nm [19] and can be used to mediate intercellular communication [20]. EPC-derived exosomes (EPC-Exos) can accelerate cutaneous wound healing [21] and ameliorate acute lung injury [22], opening a new horizon for therapeutic applications of EPC-Exos. Our previous study confirmed that EPC-Exos induce proliferation and angiogenesis of cardiac fibroblasts (CFs) and provide promising therapeutic effects for MF [23].

Emerging evidence indicates that exosomes can transport functional microRNAs (miRNAs) to induce degradation of target gene messenger RNA (mRNA) [24, 25] and play significant roles in physiology and disease [26, 27]. Circulating miRNAs can also serve as putative biomarkers of MF [28]. miRNA-enriched exosomes contribute to cardiac nuclear factor (erythroid-derived 2)-like 2 (Nrf2) dysregulation and have the potential to reduce MI-related adverse events and attenuate MI-induced myocardial injury [29]. Therefore, we hypothesized that the therapeutic effects of EPC-Exos on MF or MI may be mediated by miRNAs released from EPC-Exos.

To date, there is no reported research on the therapeutic potential of miRNAs secreted by EPC-Exos for MI. In the present study, we characterized the functional miRNAs secreted from EPC-Exos and confirmed the effects of these miRNAs on the proliferation and angiogenesis potential of CFs. In addition, the biological roles of functional miRNAs were evaluated in experimental rats with MI established via left coronary artery (LCA) ligation.

Methods

Sequence analysis of EPC-Exos miRNAs

Total RNA from EPCs and EPC-Exos was isolated by means of a mirVana miRNA isolation kit (Ambion, Austin, TX, USA). One biological repeat with three mixed samples for EPCs and EPC-Exos was used for the sequence analysis. The concentration and quality of RNA samples were detected with an Agilent 2100 Bioanalyzer (Agilent Technologies Inc., Santa Clara, CA, USA), and 50 ng RNA samples were fragmented and used for miRNA sequencing on Genome Analyzer IIx (Illumina, San Diego, CA, USA). After

generating the sequences, a BLASTN search was utilized to identify conserved miRNAs, and Rfam was employed (European Molecular Biology Laboratory, Heidelberg, Germany) for deletion of non-miRNA sequences. MiRDeep2 was used to predict novel miRNAs. The length distribution of the cells and exosomal miRNAs was analyzed, and miRNAs with differential expression between cells and exosomes were detected as described previously [30]. Gene Ontology (GO) categories [31] and Kyoto Encyclopedia of Genes and Genomes (KEGG) pathway analyses [32] were utilized to investigate specific functional roles of differentially expressed miRNAs. To determine whether the expression changes in miR-218-5p and miR-363-3p were influenced by the number of exosomes secreted from EPCs, GW4869 (an inhibitor of neutral sphingomyelinase 2, 10 μM for 12 h, MCE China) was used to treat EPCs, and then, EPC-Exos were isolated using a Total Exosome Isolation Reagent Kit (4478359, Thermo Fisher, USA).

Quantitative real-time reverse transcription-polymerase chain reaction (qRT-PCR)

Total RNA samples were extracted from EPCs, EPCs-Exos and tissues around an infarct using Trizol reagent (Takara, Dalian, Chia). The synthesis of cDNA used for gene and miRNAs was performed using a Bestar™ qPCR RT kit (DBI; #DBI-0) and Bestar™ miRNA qPCR RT kit (DBI; #2220), respectively. The relative mRNA levels of α-SMA, vimentin, CD31, VEGFR-2p53, JMY and miRNAs were determined via real-time quantitative PCR using a 20 μL reaction system. PCR was performed on an ABI PRISM 7300 real-time PCR system (Applied Biosystems, Carlsbad, CA, USA) using the following conditions: 95℃ for 2 min, followed by 40 cycles of 94℃ for 20 sec, 58℃ for 20 sec and 72℃ for 20 sec. GAPDH or U6 was used as the internal reference for genes and miRNAs, respectively. Fold changes were determined via $2^{-\Delta\Delta Ct}$ (where ΔCt = (Ct of miRNA of interest) − (Ct of U6), and ΔΔCt = (ΔCt of miRNA of interest) − (ΔCt of U6)) for at least three biological repeats with three technological replicates. All the primer sequences used are listed in Table 1.

Table 1
List of primers for qRT-PCR of the 16 differentially expressed miRNAs.

ID	Sequence (5’-3’)	Tm (°C)
U6 F	CTCGCTTCGGCAGCACA	60.42
U6 R	AACGCTTCACGAATTTGCGT	59.69
All R	CTCAACTGGTGTCGTGGA	51.5
hsa-miR-218-5p	TTGTGCTTGATCTAACCATGT	
hsa-miR-218-5p RT	CTCAACTGGTGTCGTGGAGTCGGCAATTCAGTTGAGACATGGTT	86.3
hsa-miR-218-5p F	ACACTCCAGCTGGGTTGTGCTTGATCTAACCA	75.9
hsa-miR-1-3p	TGGAATGTAAAGAAGTATGTAT	
hsa-miR-1-3p RT	CTCAACTGGTGTCGTGGAGTCGGCAATTCAGTTGAGATACATAC	82.7
hsa-miR-1-3p F	ACACTCCAGCTGGGTGGAATGTAAAGAAGTAT	70.8
hsa-miR-1246	AATGGATTTTTGGAGCAGG	
hsa-miR-1246 RT	CTCAACTGGTGTCGTGGAGTCGGCAATTCAGTTGAGCCTGCT	87.3
hsa-miR-1246 F	ACACTCCAGCTGGGAATGGATTTTTGGAGCA	77.2
hsa-miR-122-5p	TGGAGTGTGACAATGGTGTTTG	
hsa-miR-122-5p RT	CTCAACTGGTGTCGTGGAGTCGGCAATTCAGTTGAGCAAACACC	87.5
hsa-miR-122-5p F	ACACTCCAGCTGGGTGGAGTGTGACAATGGTG	78.6
hsa-miR-451a	AAACCGTTACCATTACTGAGTT	
hsa-miR-451a RT	CTCAACTGGTGTCGTGGAGTCGGCAATTCAGTTGAGAACTCAGT	85.0
hsa-miR-451a F	ACACTCCAGCTGGGAAACCGTTACCATTACTG	74.6
hsa-miR-6087	TGAGGCGGGGGGGCGAGC	
hsa-miR-6087 RT	CTCAACTGGTGTCGTGGAGTCGGCAATTCAGTTGAGGCTCGC	88.6
hsa-miR-6087 F	ACACTCCAGCTGGGTGAGGCGGGGGGGCGA	87.7
hsa-miR-363-3p	AATTGCACGGTATCCATCTGTA	
hsa-miR-363-3p RT	CTCAACTGGTGTCGTGGAGTCGGCAATTCAGTTGAGTACAGATG	84.6
hsa-miR-363-3p F	ACACTCCAGCTGGGAATTGCACGGTATCCATC	78.1
hsa-miR-486-5p	TCCTGTACTGAGCTGCCCCGAG	
hsa-miR-486-5p RT	CTCAACTGGTGTCGTGGAGTCGGCAATTCAGTTGAGCTCGGGGC	90.8
hsa-miR-486-5p F	ACACTCCAGCTGGGTCCTGTACTGAGCTGCCC	79.5

ID	Sequence (5’-3’)	Tm (°C)
hsa-miR-500a-3p	ATGCACCTGGGCAAGGATTCTG	
hsa-miR-500a-3p RT	CTCAACTGGTGTCGTGGAGTCGGCAATTCAGTTGAGCAGAATCC	87.1
hsa-miR-500a-3p F	ACACTCCAGCTGGGATGCACCTGGGCAAGGAT	82.2
hsa-miR-29b-3p	TAGCACCATTTGAAATCAGTGTT	
hsa-miR-29b-3p RT	CTCAACTGGTGTCGTGGAGTCGGCAATTCAGTTGAGAACACTGA	86.1
hsa-miR-29b-3p F	ACACTCCAGCTGGGTAGCACCATTTGAAATCA	75.7
hsa-miR-362-5p	AATCCTTGGAACCTAGGTGTGAGT	
hsa-miR-362-5p RT	CTCAACTGGTGTCGTGGAGTCGGCAATTCAGTTGAGACTCACACC	87.3
hsa-miR-362-5p F	ACACTCCAGCTGGGAATCCTTGGAACCTAGGTG	77.6
hsa-miR-221-5p	ACCTGGCATACAATGTAGATTT	
hsa-miR-221-5p RT	CTCAACTGGTGTCGTGGAGTCGGCAATTCAGTTGAGAAATCTAC	83.3
hsa-miR-221-5p F	ACACTCCAGCTGGGACCTGGCATACAATGTAG	75.4
hsa-miR-21-3p	CAACACCAGTCGATGGGCTGT	
hsa-miR-21-3p RT	CTCAACTGGTGTCGTGGAGTCGGCAATTCAGTTGAGACAGCCCA	89.0
hsa-miR-21-3p F	ACACTCCAGCTGGGCAACACCAGTCGATGGGC	83.4
hsa-miR-374a-3p	CTTATCAGATTGTATTGTAATT	
hsa-miR-374a-3p RT	CTCAACTGGTGTCGTGGAGTCGGCAATTCAGTTGAGAATTACAA	83.9
hsa-miR-374a-3p F	ACACTCCAGCTGGGCTTATCAGATTGTATTGT	71.5
hsa-miR-365a-5p	AGGGACTTTTGGGGGCAGATGTG	
hsa-miR-365a-5p RT	CTCAACTGGTGTCGTGGAGTCGGCAATTCAGTTGAGCACATCTG	87.3
hsa-miR-365a-5p F	ACACTCCAGCTGGGAGGGACTTTTGGGGGCAGA	83.3
hsa-miR-181a-3p	ACCATCGACCGTTGATTGTACC	
hsa-miR-181a-3p RT	CTCAACTGGTGTCGTGGAGTCGGCAATTCAGTTGAGGGTACAAT	85.5
hsa-miR-181a-3p F	ACACTCCAGCTGGGACCATCGACCGTTGATTG	80.4
GAPDH F	TGTTCGTCATGGGTGTGAAC	56.7
GAPDH R	ATGGCATGGACTGTGGTCAT	57.8
ACTA2 F	CCCTTGAGAAGAGTTACGAGTT	55.1
ACTA2 R	ATGATGCTGTTGTAGGTGGTT	54.5

ID	Sequence (5’-3’)	Tm (°C)
Vimentin F	CCTTGAACGCAAAGTGGAAT	57.8
Vimentin R	AGGTCAGGCTTGGAAACATC	56.4
CD31 F	CCTGCGGTATTCAAAGACAAC	57.5
CD31 R	GGGACCAGATCCTTCATTCAC	58.1
KDR F	AGAGTGGCAGTGAGCAAAGG	57.6
KDR R	CATAGACATAAATGACCGAGGC	56.9
TP53 F	CAGCACATGACGGAGGTTGT	58.8
TP53 R	TCATCCAAATACTCCACACGC	58.3
JMY F	AGCAGGAAATCGACACTCTGT	56.3
JMY R	TCCTCGGGATCATCGGTCTC	61.8

Luciferase reporter assay

Through TargetScan (http://www.targetscan.org) and the UCSC (https://genome.ucsc.edu/) website, we successfully predicted the putative targets of miR-218-5p and miR-363-3p as the p53 promoter region and the 3’ UTR of junction-mediating and regulatory protein (JMY), respectively. The interaction between the p53 promoter region and miR-218-5p, and the 3’ UTR of JMY and miR-363-5p was evaluated using a Dual-Luciferase Reporter Assay System (Promega, Madison, USA) as instructed by the manufacturer. For the p53 promoter region, wild-type and mutant sites were constructed and subcloned into pGL3-Basic vector (Promega, E1751, Madison, USA). For the 3’ UTR of JMY, wild-type and mutant sites were constructed and subcloned into psi-Check2 vector (Promega, C8021, Madison, USA). Using Lipofectamine™ 2000 transfection reagent (cat. #52887; Invitrogen, Carlsbad, USA), CFs were co-transfected with pGL3-Basic or pGL3-Basic-p53 promoter together with miR-218-5p and pRL-SV40, or CFs were co-transfected with psi-Check2 or psi-Check2-3’UTR-JMY together with miR-363-3p. *Caenorhabditis elegans* Cel-miR-39 mimic served as the negative control. Forty-eight hours after transfection, the cells were washed twice with phosphate-buffered saline and lysed using passive lysis buffer. Luciferase activity was evaluated with the Dual-Luciferase Reporter Assay System (Promega). The primers used for vector construction are listed in Table 2.

Table 2
List of primers for the wild-type and mutant promoter of p53 and 3'UTR of JMY construction in the luciferase assay.

ID	Sequence (5'-3')
JMY-P1	JMY-F1:CCGCTCGAGGCAGGTTATCACTTTCCAGTCGTTC
	JMY-R1:ATTTGCGGCCGCTAAAAGCACGGAAACTTCAAAACCT
	JMY-MUT-F1:ACATGAATTTTACATCGTGCCAGTTCCTGACTGCAAT
	JMY-MUT-R1:ATTGCAGTCAGGAACTGGCACGATGTAAAATTCATGT
JMY-P2	JMY-F2:CCGCTCGAGTAAATGATGCTACCCATACAGTGAC
	JMY-R2:ATTTGCGGCCGCAAAAGGCAACAGTCAAAACGA
	JMY-MUT-F2:CCATTTACTAGCTTTCGTACCGATTATAAAAGGTAG
	JMY-MUT-R2:CTACCTTTTATAATCGGTACGAAAGCTAGTAAATGG
TP53	TP53-F: GGGGTACCACCGAGTCCCGCGGTAATTC
	TP53-R: CCCTCGAGATCTCCTTCACAACCCTTATCACTC
	TP53-MUT-F: CCGCGGTAATTCTTATCAGCTCTGCACCGCCCC
	TP53-MUT-R: GGGGCGGTGCAGAGCTGATAAGAATTACCGCGG

Isolation of EPC-Exos, cell culture and transfection

The preparation and culture of EPCs and cardiac fibroblasts were described previously [23]. Briefly, for preparation and culture of EPCs, human peripheral blood (1:1 with phosphate-buffered saline (PBS)) was overlaid onto separation medium (GE Healthcare, Piscataway, NJ, USA) with endothelial growth factors and cytokines. The medium was centrifuged at 2,000 r/min for 30 min, and the mononuclear cells were collected. After washing with PBS, the mononuclear cells were placed into a 25 cm^2 culture bottle with DMEM (Dulbecco's modified Eagle's medium, GIBCO BRL, Grand Island, NY, USA) containing 10% FBS (fetal bovine serum, GIBCO). The FBS was pre centrifuged to remove any exosomes (100,000 g for 3 h). After 72 h, the nonadherent cells were removed, and the medium was refreshed every three days. The cells were incubated in a 37 °C constant temperature incubator with 5% CO_2. EPCs at passage 3–6 were utilized for the following experiments. For isolation of EPC-Exos, EPCs were harvested at 90% confluency, washed with PBS three times and cultured in EGM-2 (endothelial cell growth medium-2, Lonza, CC3162) containing 10% exosome-depleted FBS for 24 h. The culture medium from the EPCs was collected and centrifuged at 3,000 g for 30 min, followed by 100,000 g for 90 min at 4 °C. The supernatant was centrifuged at 100,000 g for 1 h at 4 °C to obtain the exosomes. The morphology of the exosomes was examined via transmission electron microscopy (Hitachi H-7650, Japan). For functional assays, 10,000 EPCs (in 100 μL) per well were seeded in 6-well plates for 24 h and transfected with 100 pM miRNA mimic or inhibitor of miR-6087, miR-218-5p or miR-363-3p (synthesized by GenePharma, Suzhou, China)

using Lipofectamine 2000 (Invitrogen, CA) (Table 3), and 24 h later, the EPC-Exos were isolated, and qRT-PCR detection was performed to assess transfection efficiency. A human cardiac fibroblast cell line was purchased from PriCells (HUM-CELL-0016, Wuhan, China) and cultured in DMEM with 10% FBS to remove weakly attached and unattached cells. The CFs (1×10^5 cells per well) were seeded onto 35-mm plates, cultured for three days, and then co-cultured with 0.5 μg EPC-Exos transfected with miRNA mimic or inhibitor for 48 h before further functional assays. For P53 suppression and JMY overexpression in CFs, 1×10^5 cells per well were seeded onto 35-mm plates, cultured for three days and then transfected with 2 μg si-P53 or OE-JMY and cultured for 48 h before further functional assays. si-NC and OE-NC acted as controls. In addition, the cultured CFs were transfected with 100 pM miRNA mimic or inhibitor of miR-218-5p and miR-363-3p to directly detect the role of miR-218-5p and miR-363-3p in angiogenesis and cell proliferation.

Table 3
List of miRNA mimic or inhibitor.

miRNA	Sequence
miR-218-5p mimic	5’-UUGUGCUUGAUCUAACCAUGU-3’
	3’-AUGGUUAGAUCAAGCACAAUU-5’
miR-218-5p inhibitor	5’-ACAUGGUUAGAUCAAGCACAA-3’
miR-363-3p mimic	5’-AAUUGCACGGUAUCCAUCUGUA-3’
	3’-CAGAUGGAUACCGUGCAAUUUU-5’
miR-363-3p inhibitor	5’-UACAGAUGGAUACCGUGCAAUU-3’
cel-miR-39 mimic	5'-UCACCGGGUGUAAAUCAGCUUG-3'
	3'-AGCUGAUUUACACCCGGUGAUU-5'
miR-6087 mimic	5’-UGAGGCGGGGGGGCGAGC-3’
	3’-UCGCCCCCCCGCCUCAUU-5’
miR-6087 inhibitor	5’-GCUCGCCCCCCCGCCUCA-3’

Cell proliferation assay

A volume of 100 μL containing 8,000 CFs harboring si-NC, si-p53, OE-NC or OE-JMY plasmid were co-cultured with EPC-Exos in 96-well plates for 24 h, and the cells were transfected with siRNA or plasmid for another 24 h. CCK8 (Cell Counting Kit-8) assays (Solarbio, Beijing, China) were utilized to evaluate cell viability after the addition of 0.5 μg exosomes for another 24, 48 or 72 h. Cell viabilities were calculated via measurement of optical density at 450 nm using a spectrophotometric plate reader (BioTek, USA). Cultured cells (2×10^4/mL) in a volume of 200 μL were treated with 50 μM BrdU (5-bromo-2´-deoxyuridine) labelling solution (B23151, Invitrogen, CA). The cells were incubated at 37 °C for 2 h, fixed with 4% formaldehyde in PBS for 15 min and permeabilized with Triton X-100 for another 20 min. Cells were

incubated in 1 M HCl for 10 min on ice and neutralized with 0.1 M phosphate/citric acid buffer (pH 7.4). The cells were blocked with 0.3% Triton X-100 and 10% normal goat serum for 1 h and incubated with a monoclonal rat anti-BrdU antibody (1:100, Accurate) overnight at 4 °C, followed by blocking with 5% BSA. Fluorescence-labelled secondary antibodies were added (1:1,000, Alexa Fluor 488 goat anti-rat IgG; Molecular Probes) and incubated with the cells for 1 h at room temperature. The nuclei were stained with Hoechst 33258. Immunostaining was visualized with a fluorescence microscope (Olympus inverted microscope IX71) and quantitated using flow cytometry. Cells within the field of view under the same magnification and with the same cell seeding density before the experiment were analyzed in the study.

Cell phagocytosis assay

CFs (1×10^4/mL in a volume of 100 μL) co-cultured with EPC-Exos were seeded in a 24-well plate coated with a gelatin-based coating solution (6950, Cell Biologics) for 10 min to achieve 90% confluence. The cells were washed with 1% bovine serum albumin (BSA) and incubated in culture medium containing 0.05% FBS at 37 °C for 2 h. After removal of the cell culture medium, the cells were incubated with 10 μg/mL Dil-Ac-LDL (acetylated low-density lipoprotein, labelled with 1,1-dioctadecyl-3,3,3,3-tetramethylindocarbocyanine, L-35353, Alexa 594, Life Technologies) at 37 °C for 4 h. After that, the cells were incubated with anti-Dil-Ac-LDL and anti-UAE-1 (Ulex europaeus Agglutinin I), and the staining was detected as described previously [23].

Immunofluorescence staining

The CFs co-cultured with EPC-Exos were fixed with 4% paraformaldehyde and permeabilized with 0.1% Triton X-100. After blocking with 5% BSA, the cells were incubated with the following primary antibodies: anti-α-smooth muscle actin (SMA, Abcam, ab5831), anti-vimentin (Abcam, ab92547), anti-CD31 (Dako, M0823), anti-vascular endothelial growth factor receptor 2 (VEGFR-2, Abcam, ab10972), anti-p53 (Abcam, ab131442) or anti-JMY (Abcam, ab217953) overnight at 4 °C. The cells were incubated for 30 min with the appropriate secondary antibody conjugated to fluorescein isothiocyanate (FITC). The nuclei were stained with 4',6-diamidino-2-phenylindole (DAPI, Sigma-Aldrich). Briefly, the cells were washed twice with PBS and incubated for 5 min in the dark with 1:750 solution of stock DAPI (2 mg/mL). After rinsing with PBS, the slides were allowed to air dry at room temperature, and the cells were observed under an Afv10i confocal microscope (Olympus, Japan).

Western blotting and tube-like structure formation assay

Cells and tissues were collected and snap-frozen in liquid nitrogen using the ultrasonic cell-break method for five sec on ice. After centrifugation at 12,000 g for 30 min, the supernatant was collected. Protein lysates (30 μg) were loaded onto SDS-PAGE gels and transferred to PVDF membranes. The PVDF membranes were blocked with 5% BSA and incubated overnight with monoclonal antibodies against α-SMA (1:1,000, Santa Cruz, CA, USA), vimentin (1:1,000), CD31 (1:2,000), VEGFR-2 (1:2,500), p53 (1:1,500), JMY (1:3,000), collagen-1/3 (1:2000) or Timp1-4 (1:3000). The membranes were probed with secondary antibody (1:4,000; Abcam). Immunoreactivity was determined via enhanced chemiluminescence

(Millipore, USA). Glyceraldehyde-3-phosphate dehydrogenase (GAPDH, 1:10,000) was utilized as a control.

For detection of tube-like structure formation, Matrigel (300 μL) was plated into the bottom of 6-well plates at 37 °C for 30 min, and 10,000 CFs were seeded on the Matrigel and treated with exosomes containing miRNAs for 24 h. An inverted microscope (Olympus) was used to assess tube formation.

Animal experimental model

Three-month-old healthy male SD (Sprague-Dawley) rats (230–250 g) were used for experimentation in accordance with German federal law regarding the protection of animals and the 'Guide for the Care and Use of Laboratory Animals' (National Institutes of Health publication 8th Edition, 2011). The protocol was approved by the Committee for the Ethics of Animal Experiments of The First Affiliated Hospital of Sun Yat-sen University. The rats were fixed on a board and anaesthetized via ether inhalation. Surgery was performed under sterile conditions. After non-invasive oral endotracheal intubation, we disinfected the chest of the rats and lightly pressed on the right side of the thorax, extruding the heart and inserting a needle 2 mm below the root of the left atrial appendage to a needle depth of 0.5 mm. We threaded the surface of the myocardium near the pulmonary arterial cone with 6/0 suture, rapidly ligated the left anterior descending artery, closed the thorax and finally sutured the incisions layer by layer. The rats were allowed to move freely after surgery and were injected with 400,000 U penicillin to prevent infection. Post-operative medication was also used to alleviate any discomfort.

After the operation, when the animals recovered spontaneous breathing, rats whose electrocardiogram (ECG) showed significantly increased J points and/or tall and biphasic or inverted T waves and/or Q waves were considered to be MI rats. The animals that met the above ECG requirements were randomly divided into three groups: MI group (model), MI with exosomes containing miR-218-5p mimic group and MI with exosomes containing miR-363-3p mimic group, with ten rats in each group. Pooled exosomes containing miR-218-5p mimic or miR-363-3p mimic (300 μg) were first resuspended in 150 μL of PBS and injected intramyocardially with an insulin syringe through a 21-gauge needle into the border of the visually recognizable ischemic area at 24 h after surgery. The sham operated group without any surgery and the control model rats were injected with 150 μL of PBS. After eight weeks, echocardiography was used to detect cardiac function in the rats. Capillary density was observed and calculated under an optical microscope.

Histological Evaluation

The heart tissues of rats in the different groups were immediately dissected, fixed in 10% buffered formalin and processed in a paraffin tissue processing machine. Seven-micrometer sections were stained with hematoxylin and eosin (H&E, G1005, Servicebio, China), Masson's trichrome (G1006, Servicebio, China) and Van Gieson (G1046, Servicebio, China), and the tissues were assessed. Representative photomicrographs were observed under a microscope. For measurement of infarct volumes, the excised left ventricles of the hearts were frozen and sectioned from the apex to the base into 3 mm slices. The slices were immersed in 2% TTC (2,3,5-triphenyltetrazolium chloride, T8877, Sigma-Aldrich) solution in

PBS for 30 min at 37 °C in the dark. The slices were fixed in 10% formaldehyde, and the area of the ischemic damage was measured using a morphometric program (Digi Cell 4.0).

Immunohistochemistry

Heart tissues slices were blocked by incubation with 3% H_2O_2 after deparaffinization and rehydration and washed with 0.05 M ethylenediaminetetraacetic acid (EDTA) followed by 4% paraformaldehyde. The tissues were incubated in 5% dry milk and 0.5% goat serum for 20 min. Then, 5 μm sections were incubated with anti-von Willebrand factor (anti-vWF) antibody in the presence of 10% rabbit serum overnight at room temperature. The sections were incubated with horseradish peroxidase (HRP)-conjugated goat anti-rabbit IgG secondary antibody for another two hours. Diaminobenzidine (DAB) staining (K5007, DAKO) was used for examination. The slides were counterstained with Harris hematoxylin to stain cell nuclei. The heart tissue slices were also incubated with anti-α-SMA antibody and the respective secondary antibody. The slides were counterstained with DAPI to stain cell nuclei.

Statistical Analysis

All the data are presented as the means ± standard deviation (SD). Each *in vitro* experiment was performed in triplicate. All the data produced by qRT-PCR were based on at least 3 biological repeats with at least 3 technical repeats. Statistical significance between/among different treatment groups was calculated using one-way analysis of variance (ANOVA) followed by Dunnett's multiple comparison test or an unpaired Student t-test, as appropriate, using SPSS 19.0 software (SPSS Inc., Chicago, IL, USA). $P < 0.05$ was considered to be statistically significant.

Results

Overview of small RNA EPC and EPC-Exos sequencing data

A previous study demonstrated that EPC-Exos play a vital role in CF proliferation and angiogenesis [23]. To investigate similarities or differences in specific patterns of miRNA expression between cells and exosomes, we first isolated exosomes and identified them via transmission electron microscopy (**Supplemental Fig. 1A**), particle diameter size distribution (**Supplemental Fig. 1B**), western blot analysis (**Supplemental Fig. 1C**) and PKH67 staining (**Supplemental Fig. 1D**). In an initial effort to identify differentially expressed miRNAs in exosomes that could account for their functions relative to EPCs, we profiled the expression of miRNAs using DESeq2. A total of 7,342, 859 and 8,898,449 clean reads were obtained with 6,997,238 and 8,813,698 adapter-trimmed reads (length ≥ 15 nucleotides) from EPCs and exosomes, respectively (**Supplemental Table 1**). Further analysis showed that the number of reads aligned to known human pre-miRNAs in miRbase21 was 4,691,984 and 127,888 in EPCs and exosomes, respectively (**Supplemental Table 1**). Unique small RNAs with lengths ranging from 16–30 nucleotides were obtained by filtering the low-quality reads or sequence reads with a length less than 15 nucleotides, and the length distribution of unique small RNA sequences (17–30 nucleotides) in the cells and exosomes were similar (**Supplemental Fig. 2A**). The lengths of unique small RNAs in the cells and

exosomes ranged between 20–24 nucleotides, with the most abundant size class being 22 nucleotides followed by 23 and 21 nucleotides (**Supplemental Fig. 2A**). The new miRNAs were discovered using miRDeep2 [33]. Reads with a removed adaptor, sequence length > or = 17 base pairs and mismatch number < or = 1 were used to perform novel miRNA prediction, and 144 novel miRNA candidates were detected in chromosomes of both cell types and exosomes (**Supplemental Fig. 2B and Supplemental Table 2**).

Differential miRNA expression profile between EPCs and EPC-Exos

In total, 385 differentially expressed miRNAs were found in EPC-Exos compared with EPCs. Among these miRNAs, 100 were upregulated, and 285 were downregulated. A heat map of the hierarchical clustering of differential expression between EPCs and EPC-Exos was generated with a cut-off log2 (fold-change) > 1 and $P < 0.05$ (Fig. 1A). The top 25 upregulated miRNAs and top 25 downregulated miRNAs in the exosomes group compared with EPCs are listed in Fig. 1B. Moreover, in an attempt to validate the reliability and robustness of the miRNA sequencing results, 16 differentially expressed miRNAs (eight upregulated: miR-1246, miR-122-5p, miR-451a, miR-6087, miR-363-3p, miR-486-5p, miR-218-5p, and miR-1-3p and eight downregulated: miR-181-3p, miR-500a-3p, miR-362-5p, miR-21-3p, miR-374a-3p and miR-365a-5p in EPC-Exos) were selected and analyzed via qRT-PCR. The qRT-PCR results showed that miR-1246, miR-122-5p, miR-451a, miR-6087, miR-363-3p, miR-486-5p and miR-218-5p were upregulated while miR-181-3p, miR-500a-3p, miR-362-5p, miR-21-3p, miR-374a-3p and miR-365a-5p were downregulated in EPC-Exos compared with EPCs (Fig. 1C). Furthermore, KEGG pathway analysis showed that upregulated miRNAs were significantly enriched in *Salmonella* infection, the HIF-1 signaling pathway and cancer pathways, while downregulated miRNAs were significantly enriched in protein digestion and absorption, focal adhesions and cancer pathways (**Supplemental Fig. 3A**). Moreover, Gene Ontology (GO) analysis was performed to identify the key genes targeted by specific miRNAs. Upregulated miRNAs mainly participated in ion transport, regulation of anoikis and neuromuscular functions (**Supplemental Fig. 3B**), while downregulated miRNAs mainly participated in collagen and multicellular organism catabolic processes (**Supplemental Fig. 3C**) for biological process (BP), cellular component (CC) and molecular function (MF).

miR-218-5p and miR-363-3p promote CF angiogenesis and proliferation

To investigate the functional potential of miRNAs in MF, three miRNAs, namely, miR-6087, miR-218-5p and miR-363-3p, which showed the most significant changes in the expression profiles, were selected for further examination. EPCs were transfected with mimics and inhibitors of the miRNAs, and their expression levels were detected in EPC-Exos using qRT-PCR (Fig. 2A). The expression of miR-218-5p and miR-363-3p was significantly upregulated with miRNA mimic transfection and downregulated with miRNA inhibitor transfection in EPC-Exos compared with the NC-Exo group (Fig. 2A). However, the expression of miR-6087 was not affected (Fig. 2A). To determine whether the expression changes in miR-

218-5p and miR-363-3p were caused by the number of exosomes secreted from EPCs, GW4869 (an inhibitor of neutral sphingomyelinase 2) was used to treat EPCs. As shown in **Supplemental Fig. 4A and 4B**, the concentration of exosomes in EPCs treated with GW4869 was significantly decreased compared with the control. Further analysis showed that the expression of miR-218-5p and miR-363-3p was significantly increased in cells treated with GW4869 compared with control cells but significantly decreased in EPC-Exos (**Supplemental Fig. 4C and 4D**). Therefore, miR-218-5p and miR-363-3p were selected for further experiments.

To investigate whether the two candidate miRNAs are involved in mediation of CF proliferation and angiogenesis, CFs (NC-Exo), CFs + EPC-Exos with miR-218-5p mimic (mimic-218-Exo), CFs + EPC-Exos with miR-218-5p inhibitor (inhibitor-218-Exo), CFs + EPC-Exos with miR-363-3p mimic (mimic-363-Exo) and CFs + EPC-Exos with miR-363-3p inhibitor (inhibitor-363-Exo) were established. The number of capillary-like structures was increased in the mimic-218-Exo and mimic-363-Exo groups compared with the NC-Exo group and was decreased in the inhibitor-218-Exo and inhibitor-363-Exo groups (Fig. 2B). Further analysis showed that the tube length in CFs with miRNA mimic-Exo transfection was significantly longer than that in the control, while shorter tube lengths were observed in the miRNA inhibitor-Exo groups (Fig. 2B). These results indicate that miR-218-5p and miR-363-3p can promote angiogenesis of CFs. CCK-8 assays demonstrated that treatment with miR-218-5p and miR-363-3p mimic-Exo dramatically increased cell viability compared to the control, while miRNA inhibitor-Exo significantly decreased cell viability at 48 h and 72 h (Fig. 2C). These findings suggest that miR-218-5p and miR-363-3p can promote CF proliferation. To verify the results of this experiment, we performed a BrdU labelling assay. The results confirmed that EPC-Exos with miRNA mimic significantly promoted the proliferation of CFs, because the number of BrdU-positive cells found in CFs treated with mimics was greater than that in the inhibitor and control groups (Fig. 2D). Therefore, miR-218-5p and miR-363-3p promoted CF proliferation.

In order to further confirm that miR-218-5p and miR-363-3p which play important roles in CF proliferation and angiogenesis related to EPC-exo, the function analysis of EPC-exo to CF proliferation and angiogenesis was performed in a co-culture system. CCK-8 assays showed that cell viability was dramatically increased in Exo group compared with control while significantly decreased when treated with GW4869 compared with Exo group at 48 h (**Supplemental Fig. 5A**). Further analysis showed that the number of capillary-like structures and the tube length in CFs was increased in Exo group compared with control while decreased when treated with GW4869 compared with Exo group (**Supplemental Fig. 5B**). These results demonstrated that miR-218-5p and miR-363-3p which promoted CF proliferation and angiogenesis were from EPC-exo.

To further confirm the changes in CF angiogenesis and proliferation caused by miR-218-5p and miR-363-3p, CFs were directly transfected with miR-218-5p and miR-363-3p. miR-218-5p and miR-363-3p were successfully overexpressed or suppressed in CFs harboring mimic or inhibitor, respectively (**Supplemental Fig. 6A**). Further analysis showed that the expression of p53 was significantly upregulated in the mimic-218 (miR-218-5p mimic) group and downregulated in the inhibitor-218 (miR-218-5p inhibitor) group compared with the NC group. In addition, the expression of JMY was significantly downregulated in the

mimic-363 (miR-363-3p mimic) group but upregulated in the inhibitor-363 (miR-363-3p inhibitor) group compared with the NC group (**Supplemental Fig. 6B**). In addition, the results showed that tube length was significantly elevated in both the mimic-218 and mimic-363 groups and decreased in the inhibitor group compared with the NC group (**Supplemental Fig. 6C and 6D**). BrdU labelling showed that the number of BrdU-positive cells found in CFs treated with mimic-218 or mimic-363 was more than that in the control groups, while the number in the inhibitor-treated group was decreased (**Supplemental Fig. 6E and 6F**).

miR-218-5p and miR-363-3p promoted mesenchymal-endothelial transition in CFs

In our previous study, we demonstrated that EPC-Exos promoted mesenchymal-endothelial transition (MEndT) to reduce MF [23]. To test the functional potential of miR-218-5p and miR-363-3p in MEndT, we detected the specific endothelial lineage characteristics of CFs using a phagocytosis assay. The results showed that phagocytosis in CFs dramatically increased in the mimic-218-Exo group (Fig. 3A) and mimic-363-Exo group (Fig. 3B) in comparison with the NC-Exo group and inhibitor-Exo group. We also assessed the expression of the endothelial cell markers cluster of differentiation 31 (CD31) and vascular endothelial growth factor receptor 2 (VEGFR-2) and the mesenchymal cell markers alpha smooth muscle actin (α-SMA) and vimentin. qRT-PCR analysis showed that the expression of α-SMA and vimentin were significantly downregulated in the mimic-218-Exo group (Fig. 3C) and mimic-363-Exo group (Fig. 3D), while the expression levels of CD31 and VEGFR-2 were upregulated compared to the NC-Exo group and inhibitor-Exo group (Fig. 3C and 3D). Immunofluorescence staining (Fig. 4A-D) and western blot analysis (Fig. 5A and 5B) showed a decrease in the fibrosis markers α-SMA and vimentin and an increase in the endothelial markers CD31 and VEGFR-2 in the mimic-218-Exo and mimic-363-Exo groups. However, the opposite effects on the expression of these proteins were observed in the inhibitor-Exo groups. Transfection with miR-218-5p and miR-363-3p mimics induced MEndT in CFs, thereby playing an important role in ameliorating MF.

p53/JMY were respective targets of miR-218-5p and miR-363-3p

To investigate the molecular mechanism of the miR-218-5p- and miR-363-3p-mediated effects on MF, we utilized TargetScan to identify the potential binding sites of miR-218-5p and miR-363-3p. Systematic bioinformatics analysis revealed that miR-218-5p could bind with the 5’-AAGCAC-3’ site in the promoter region of P53 and that miR-363-3p could bind with the 5’-GUGCAAU-3’ site in the 3’UTR of JMY mRNA at two sites (Fig. 6A and 6D). Therefore, a luciferase reporter assay was used to identify interactions between miR-218-5p and the P53 promoter, and miR-363-3p and the 3’UTR of JMY. No obvious changes were observed in the NC and cel-miR-39 mimic groups, which harbored the wild-type and mutant P53 promoter. However, luciferase activity was significantly upregulated after co-transfection with miR-218-5p mimic and the reporter vector with the wild-type P53 promoter, while no significant change was observed with the mutant P53 promoter (Fig. 6B and 6C). In addition, no obvious changes were found in the NC and cel-miR-39 mimic groups, harboring the wild-type and mutant JMY 3’ UTR, regardless of whether the

P1 or P2 binding site was present. However, luciferase activity was significantly decreased after co-transfection with miR-363-3p mimic and the reporter vector with wild-type JMY at the P2 binding site, while no significant change was observed for the P1 binding site (Fig. 6E and 6F). Therefore, miR-218-5p could bind the p53 promoter region, and miR-363-3p could bind P2 sites in the 3' UTR of JMY.

Furthermore, the mRNA expression of *TP53 (P53)* was upregulated in the mimic-218-Exo group and downregulated in the inhibitor-Exo group compared to the NC-Exo group (Fig. 6G). Moreover, the mRNA expression of JMY was significantly downregulated in the mimic-363-Exo group and upregulated in the inhibitor-Exo group compared with the NC-Exo group (Fig. 6G). The expression changes in TP53 and JMY were further verified by immunofluorescence staining (Fig. 7A and 7C) and western blot analysis (Fig. 7B and 7D). In addition, the expression of p53 was suppressed and JMY was overexpressed in CFs (Fig. 7E) compared with the mimic-218-Exo and Mimic-363-Exo groups, respectively. We also found that both tube length (Fig. 7F) and the number of BrdU-positive cells (Fig. 7G) were dramatically decreased in both the si-p53 and OE-JMY group compared with the mimic-218-Exo and mimic-363-Exo group, respectively. In general, our results indicate that EPC-Exos regulate the proliferation, angiogenesis and tube formation of CFs through miR-218-5p- and miR-363-3p-mediated p53 /JMY signaling pathways.

miR-218-5p and miR-363-3p mimic alleviated LCA ligation-induced MI

To investigate whether exosomal miR-218-5p and miR-363-3p can ameliorate LCA ligation-induced MI *in vivo*, we first constructed a MI rat model by injecting EPC-Exos containing miR-218-5p and miR-363-3p mimic. ECGs showed inverted QRS waves in the MI model group (Model) compared to the sham-operated group (Sham), suggesting successful establishment of an MI model (Fig. 8A). Injection of EPC-Exos with miR-218-5p and miR-363-3p mimic nearly reversed the arrhythmia, indicating a therapeutic effect on MI (Fig. 8A). Furthermore, LVEDd, LVESd and LVIDs were increased in the Model group, and these effects were partially reversed by treatment with EPC-Exos containing miR-218-5p and miR-363-3p mimic (Table 4). Similarly, the decreased parameter values in the Model rats, including HR, LVIDd, SV, LVEF, FS, CO, LVPWT and LVAWT, were also partially restored to the values seen in Sham rats after treatment with EPC-Exos containing miR-218-5p and miR-363-3p mimic (Table 4). For TTC staining, a large core volume of tissue injury was found in the Model group (Fig. 8B). However, the core volume steadily decreased to approximately 50% in the mimic-218-Exo and mimic-363-Exo groups compared with the model group (Fig. 8B). Subsequently, significant increased expression of miR-218 and miR-363 was observed both in the Mimic-363-Exo and Mimic-218-Exo group compared with Sham and Model group (Fig. 8C). Furthermore, we found that the expression of JMY was significantly decreased in the Mimic-363-Exo group while the expression of p53 was significantly elevated in the Mimic-218-Exo group compared with the model group (Fig. 8D and 8E). Western blotting also confirmed these results (Fig. 8F). In addition, we detected the expression of collagen-1, collagen-3, Timp-1, Timp-2, Timp-3 and Timp-4. As shown **in** Fig. 8F, the expression levels of collagen-1 and collagen-3 were significantly decreased, while those of Timp-1 and Timp-3 were upregulated (no change in the expression of Timp-2 and Timp-4) in both the

Mimic-218-Exo and Mimic-363-Exo groups compared with the model group (Fig. 8F). Therefore, exosomal miR-218-5p and miR-363-3p can reduce cardiac dysfunction in MI rats.

Table 4 Effect of EPC-Exos with miR-218-5p and miR-363-3p mimic on the cardiac ultrasonography index of LCA ligation-induced myocardial infarction rats.

Groups	Sham	Model	mimic-218-Exo	mimic-363-Exo
HR (bpm)	333 ± 11.6	265 ± 13.9	314 ± 13.9 (p = 0.555)	315 ± 16.5 (p = 0.532)
LVESd (mm)	3.741 ± 0.103	5.226 ± 0.221	4.593 ± 0.276 (p = 0.598)	4.325 ± 0.215 (p = 0.515)
LVEDd (mm)	5.954 ± 0.297	7.023 ± 0.265	6.483 ± 0.293 (p = 0.810)	6.443 ± 0.331 (p = 0.767)
LVIDs (μL)	94.103 ± 2.084	108.871 ± 1.740	102.014 ± 1.972 (p = 0.878)	94.874 ± 2.256 (p = 0.656)
LVIDd (μL)	246.593 ± 12.001	217.715 ± 7.273	224.714 ± 10.788 (p = 0.899)	231.734 ± 7.194 (p = 0.766)
SV (μL)	152.49 ± 2.990	108.844 ± 1.787	122.7 ± 4.865 (p = 0.599)	136.86 ± 2.487 (p = 0.419)
LVEF (%)	73.812 ± 1.852	52.994 ± 1.829	60.488 ± 2.648 (p = 0.633)	65.192 ± 2.522 (p = 0.472)
FS (%)	37.168 ± 2.620	25.587 ± 2.528	29.153 ± 2.420 (p = 0.719)	32.872 ± 1.444 (p = 0.473)
CO (mL/min)	50.77917 ± 2.486	28.84366 ± 1.986	38.5278 ± 1.272 (p = 0.305)	43.1109 ± 2.048 (p = 0.515)
LVPWT (mm)	2.215 ± 0.112	2.208 ± 0.138	2.227 ± 0.109 (p = 0.882)	2.209 ± 0.131 (p = 0.793)
LVAWT (mm)	2.224 ± 0.153	1.762 ± 0.124	1.969 ± 0.147 (p = 0.469)	2.073 ± 0.163 (p = 0.526)

Note: HR: heart rate; bpm: beat per minute; LVESd: left ventricular end systolic diameter; LVEDd: left ventricular end diastolic diameter; LVIDs: left ventricular internal diameter end systole; LVIDd: left ventricular internal diameter end diastole; SV: stroke volume; LVEF: left ventricular ejection fraction; FS: fractional shortening; CO: cardiac output; LVPWT: left ventricular posterior wall thickness; LVAWT: left ventricular anterior wall thickness. The P value refers to mimic-218-Exo or mimic-363-Exo vs. the model group.

Histological examination of the rat heart tissues was further performed. As shown in Fig. 9A, after the challenge of the LCA ligation, H&E staining of heart tissues showed typical MI pathological traits. However, these histopathological changes were clearly attenuated in the mimic-218-Exo and mimic-363-Exo groups, reflected by visible fibers with cross-linked-shaped striated muscle tissue containing nuclei located on the periphery of the cell and remodeling of the intercalated disc connections (Fig. 9A). Masson and Van Gieson staining confirmed a reduced degree of cardiac fibrosis with downregulation of collagen expression in the mimic-218-Exo and mimic-363-Exo groups (Fig. 9A). Moreover, the expression of α-SMA

was dramatically reduced in the mimic-218-Exo and mimic-363-Exo groups compared to the model group (Fig. 9B). Furthermore, immunohistochemistry assays showed that the von Willebrand factor (vWF) expression level was partially restored in the mimic-218-Exo and mimic-363-Exo groups compared to the model group (Fig. 9C). As a risk factor for patients with MI, vWF plays a vital role in hemostasis and is always elevated in the MI rat model [34]. We also quantified capillary density. In line with the histological examinations, the number of vessels/field area in the remodeled left ventricle in the mimic-218-Exo and mimic-363-Exo groups was increased compared with that in the model group (Fig. 9D). These findings confirm that exosomal miR-218-5p and miR-363-3p can alleviate LCA ligation-induced MI.

Discussion

Cardiovascular disease not only places a severe burden on affected patients and their families but also influences society and economic development, underscoring the need for innovative new therapies [35]. Myocardial infarction-induced remodeling of the left ventricle is the most common cause of CHF, which is the leading cause of cardiovascular mortality [1]. Therefore, exploring the regulation mechanisms underlying MI is of great significance for control of cardiovascular disease development. Accumulating evidence has shown that exosomes can play a role in therapeutic effects in MI and that miRNA plays an important role in MI [36–38]. However, the molecular mechanism of EPC-Exos miRNAs in MI is rarely studied. Here, we examined the role of exosome-derived miRNA in regulating angiogenesis, proliferation and mesenchymal-endothelial transition of CFs during MI *in vitro* and *in vivo*. The results showed that exosomal miR-218-5p and miR-363-3p from endothelial progenitor cells promoted angiogenesis, proliferation and mesenchymal-endothelial transition of CFs by targeting the p53 promoter and JMY 3'UTR, respectively, which further alleviated LCA-induced chronic myocardial infarction. Our study will shed new light on Exo-miRNA-based therapy for MI.

MicroRNAs (miRNAs) are small noncoding RNAs that block translation or induce degradation of mRNA and thereby control patterns of gene expression. Increasing studies have found that miRNAs plays crucial roles in MI [39–41]. For example, microRNA-133 overexpression promotes the therapeutic efficacy of mesenchymal stem cells in acute myocardial infarction [42]; Li et al. demonstrated that intravenous miR-144 reduces left ventricular remodeling after myocardial infarction [43]. miR-208, miR-494, miR-499 and miR-1303 expression levels are considered to be biomarkers in early diagnosis of acute myocardial infarction [44]. microRNA-21 was fund to mediates the protective effect of cardiomyocyte-derived conditioned medium on ameliorating myocardial infarction in rats [45]. These results demonstrate that different miRNAs play important roles in MI. As small nanometer-sized vesicles and intercellular shuttles, exosomes essentially transfer loading proteins and RNAs for offloading in target cells and modulate gene and protein expression, thereby regulating cell activity [37, 46]. And Luo et al. revealed that exosomes from miR-126-overexpressing ADSCS were therapeutic in relieving acute myocardial ischemic injury [47]. Tian et al. demonstrated that MI-induced microRNA-enriched exosomes contribute to cardiac Nrf2 dysregulation in chronic heart failure [29]. Zhu et al. found that hypoxia-elicited mesenchymal stem cell-derived exosomes facilitated cardiac repair through miR-125b-mediated prevention of cell death in myocardial infarction [48]. Recently, it showed that serum exosomal microrna-21, microrna-126, and pten

are novel biomarkers for diagnosis of acute coronary syndrome [49]. These results demonstrate that exosomal miRNA plays key roles in MI and might provide a novel therapeutic pathway for relieving MI. In the present study, 385 differentially expressed miRNAs, with 100 upregulated and 285 downregulated, were found in EPC-Exos compared with EPCs by sequencing and profiling miRNA expression in EPC-Exos. miR-218-5p and miR-363-3p showed the most significant changes in the expression profiles, demonstrating the important roles of miR-218-5p and miR-363-3p in MI.

Several miRNAs have been shown to control important processes that contribute to the pathophysiological consequences of MI, such as regulating cardiomyocyte cell death and postischemic neovascularization, controlling cardiomyocyte proliferation or interfering with cardioprotective effects mediated by stem or progenitor cells [50–52]. In addition, miRNAs can be used for direct reprogramming of cardiac fibroblasts into cardiomyocytes [36]. A recent study showed that EPC-Exos contribute to CF proliferation and angiogenesis and ameliorate MF [23]. Arif et al. revealed that MicroRNA-210-mediated proliferation, survival, and angiogenesis promoted cardiac repair post myocardial infarction in rodents [53]. Cardiomyocyte-derived exosomal microRNA-92a mediated post-ischemic myofibroblast activation both *in vitro* and *ex vivo* [54]. In addition, Fan et al. demonstrated that MicroRNA-210 promotes angiogenesis in acute myocardial infarction [55]; M1-like macrophage-derived exosomes suppressed angiogenesis and exacerbate cardiac dysfunction in a myocardial infarction microenvironment [56]. Ma et al. revealed that MicroRNA-132 delivered by mesenchymal stem cell-derived exosomes can promote angiogenesis in MI [57]. Therefore, we speculated that miR-218-5p and miR-363-3p might be involved in CF proliferation and angiogenesis in MI. Consistent with this hypothesis, our study revealed that miR-218-5p and miR-363-3p mimics promoted angiogenesis and proliferation in CFs. In our previous study, we demonstrated that EPC-Exos promoted mesenchymal-endothelial transition (MEndT) to reduce MF [23]. In addition, Bayoumi et al. demonstrated that microRNA-532 protects the heart in acute myocardial infarction via endothelial-to-mesenchymal transition by suppressing prss23 [58]. Our *in vivo* and *in vitro* experiments showed that miR-218-5p and miR-363-3p induced MEndT of CFs via upregulation of endothelial cell markers (CD31 and VEGFR-2) and downregulation of fibrosis markers (α-SMA and vimentin). These results demonstrate that miR-218-5p and miR-363-3p mimics promoted CF angiogenesis and proliferation by promoting mesenchymal-endothelial transition in CFs.

Increasing numbers of targets regulated by miRNAs have been reported in MI, such as PPAR-γ, Smad7, bak1, klf13 and TXNIP [59–61]. In the present study, we found that p53 and JMY were directly regulated by miR-218-5p and miR-363-3p. In addition, miR-218-5p was found to activate p53 expression, and these results are consistent with previous research [62]. P53 and JMY have been demonstrated to participate in angiogenesis and proliferation in many diseases, especially in cancer [63–65]. However, the function of p53 and JMY in MI is rarely studied. In the present study, we found that suppression of P53 and overexpression of JMY could attenuate the CF angiogenesis and proliferation affected by miR-218-5p and miR-363-3p. In addition, evidence from other groups has shown a switch regulation between p53 and MEndT in CFs, which in the absence of p53 reduces the formation of fibroblast-derived endothelial cells and leads to cardiac injury, while activation of p53 promotes MEndT, resulting in cardiac function improvement [66]. Interestingly, in addition to the involvement of transcription co-factors in the p53

signaling pathway, JMY decreases the expression of adhesion molecules in the cadherin family and contributes to assembly of the actin cytoskeleton and to nucleation of new filaments [67]. Cadherins are endothelial-specific markers, and thus, a decrease in cadherin expression reflects a decrease in endothelial -mesenchymal transition (EMT) [23]. Taken together, these results demonstrate that upregulation of p53 by miR-218-5p and downregulation of JMY by miR-363-3p might relieve MF by inducing MEndT.

In addition, we identified the effect of exosomal miR-218-5p and miR-363-3p in MI by constructing an LCA ligation-induced MI rat model. The results indicated that arrhythmia, LVEDd, LVESd, LVIDs, HR, LVIDd, SV, LVEF, FS, CO, LVPWT and LVAWT were partially restored by injection of EPC-Exos containing miR-218-5p and miR-363-3p mimic. Further analysis showed that EPC-Exos containing miR-218-5p and miR-363-3p mimic effectively suppressed infarction-induced myocardial damage by inhibiting inflammation and macrophage infiltration, downregulating collagen expression, and increasing capillary density, as shown by by histochemical staining and analysis of collagen 1, collagen 3 and Timp 1–4 expression. These results demonstrate that exosomal miR-218-5p and miR-363-3p can reduce the cardiac dysfunction in MI rats and might provide new targets for MI therapy. However, future animal studies are required to guidance administration of miR-218-5p and miR-363-3p mimic to treat MI in the clinical context. Furthermore, the specific synthesis mechanism and function of exosomes are not very detailed and there is a lack of cost-effective exosome separation technology. In addition, future studies need to classify whether miRNA packaging into exosomes and exosomal uptake is a selective/stimulus dependent process because of there is no evidence to suggest functional differences between exosomal miRNAs and free ones and whether exosomal and free miRNAs are differentially regulated in response to stimulation. However, although the current biology of exosomes is still immature, more and more interest and capital investment will accelerate the progress of basic research and clinical transformation of exosomes.

Conclusions

Our study shows that EPC-Exos containing miR-218-5p and miR-363-3p mimic exerted a protective effect against MI-induced myocardial damage and MF. Our *in vitro* results indicate that miR-218-5p and miR-363-3p mimic have protective properties against MF by targeting p53/JMY-mediated cell apoptosis and MEndT (**Figure 10**). The present study provides novel insight into the molecular mechanism underlying the effect of EPC-Exos containing miR-218-5p and miR-363-3p mimic on attenuation of myocardial damage.

Abbreviations

myocardial infarction (MI); endothelial progenitor cell-derived exosomes (EPC-Exos); myocardial fibrosis (MF); cardiac fibroblasts (CFs); microRNAs (miRNAs); quantitative real-time polymerase chain reaction (qRT-PCR); junction-mediating and regulatory protein (JMY); left coronary artery (LCA); endothelial progenitor cells (EPCs); chronic heart failure (CHF); left ventricle (LV); mesenchymal-endothelial transition

(MEndT); endothelial-mesenchymal transition (EMT); messenger RNA (mRNA); nuclear factor (erythroid-derived 2)-like 2 (Nrf2); Gene Ontology (GO); Kyoto Encyclopedia of Genes and Genomes (KEGG); Dil-Ac-LDL (acetylated low density lipoprotein, labelled with 1,1-dioctadecyl-3,3,3,3-tetramethylindocarbocyanine); CD31 (cluster of differentiation 31); BrdU (5-bromo-2´-deoxyuridine); Cell Counting Kit-8 (CCK8); UAE-1 (Ulex europaeus agglutinin I); phosphate-buffered saline (PBS); endothelial cell growth medium-2 (EGM-2); Dulbecco's modified Eagle's medium (DMEM); fetal bovine serum (FBS); α-smooth muscle actin (α-SMA); vascular endothelial growth factor receptor 2 (VEGFR-2); fluorescein isothiocyanate (FITC); 4',6-diamidino-2-phenylindole (DAPI); Tris-buffered saline-Tween-20 (TBST); glyceraldehyde-3-phosphate dehydrogenase (GAPDH); Sprague-Dawley (SD); electrocardiogram (ECG); hematoxylin and eosin (H&E); 2,3,5-triphenyltetrazolium chloride (TTC); ethylenediaminetetraacetic acid (EDTA); von Willebrand factor (vWF); horseradish peroxidase (HRP); diaminobenzidine (DAB); heart rate (HR); beat per minute (bpm); left ventricular end systolic diameter (LVESd); left ventricular end diastolic diameter (LVEDd); left ventricular internal diameter end systole (LVIDs); left ventricular internal diameter end diastole (LVIDd); stroke volume (SV); left ventricular ejection fraction (LVEF); fractional shortening (FS); cardiac output (CO); left ventricular posterior wall thickness (LVPWT); left ventricular anterior wall thickness (LVAWT)

Declarations

Ethics approval and consent to participate

The animal protocol was approved by the Committee for the Ethics of Animal Experiments of The First Affiliated Hospital of Sun Yat-sen University.

Consent for publication

N/A.

Availability of data and materials

The datasets supporting the conclusions of this article are included within the article and its additional files.

Competing interests

The authors report no conflicts of interest.

Funding

This work was supported by the Science and Technology project of Guangzhou (201604020129), the National Natural Science Foundation of China (81700263) and grants from the Natural Science Foundation of Guangdong Province (2019A1515010329 and 2018A030313782). The funders had no role in the design or conduct of the study; collection, management, analysis, and interpretation of the data;

preparation, review, or approval of the manuscript; or the decision to submit the manuscript for publication.

Authors' Contributions

Xiao Ke, Rongfeng Yang, Xun Hu and Chengheng Hu conceived and designed the experiments.

Fang Wu, Xing Wang and Jiawen Liang performed the experiments, provided new tools/reagents and analyzed the data.

Xiao Ke, Rongfeng Yang, Xun Hu and Chengheng Hu wrote the manuscript and made manuscript revisions.

All authors read and approved the final manuscript.

Acknowledgments

We appreciate Dr. Fang Yang's efforts in critically revising our paper.

References

1. Palagyi A, de Silva HA, Praveen D, Patel A: Combatting the Global Crisis of Cardiovascular Disease.*Heart Lung Circ* 2019, 28:981-983.
2. Gheorghiade M, Bonow RO: Chronic heart failure in the United States: a manifestation of coronary artery disease.*Circulation* 1998, 97:282-289.
3. Gheorghiade M, Sopko G, De Luca L, Velazquez EJ, Parker JD, Binkley PF, Sadowski Z, Golba KS, Prior DL, Rouleau JL, Bonow RO: Navigating the crossroads of coronary artery disease and heart failure.*Circulation* 2006, 114:1202-1213.
4. Mezzaroma E, Toldo S, Farkas D, Seropian IM, Van Tassell BW, Salloum FN, Kannan HR, Menna AC, Voelkel NF, Abbate A: The inflammasome promotes adverse cardiac remodeling following acute myocardial infarction in the mouse.*Proc Natl Acad Sci U S A* 2011, 108:19725-19730.
5. Song M, Jang H, Lee J, Kim JH, Kim SH, Sun K, Park Y: Regeneration of chronic myocardial infarction by injectable hydrogels containing stem cell homing factor SDF-1 and angiogenic peptide Ac-SDKP.*Biomaterials* 2014, 35:2436-2445.
6. Swynghedauw B: Molecular mechanisms of myocardial remodeling.*Physiol Rev* 1999, 79:215-262.
7. Jugdutt BI: Ventricular remodeling after infarction and the extracellular collagen matrix: when is enough enough?*Circulation* 2003, 108:1395-1403.
8. Cohn JN, Ferrari R, Sharpe N: Cardiac remodeling--concepts and clinical implications: a consensus paper from an international forum on cardiac remodeling. Behalf of an International Forum on Cardiac Remodeling.*J Am Coll Cardiol* 2000, 35:569-582.

9. Gourdie RG, Dimmeler S, Kohl P: Novel therapeutic strategies targeting fibroblasts and fibrosis in heart disease.*Nat Rev Drug Discov* 2016, 15:620-638.
10. Tao A, Song J, Lan T, Xu X, Kvietys P, Kao R, Martin C, Rui T: Cardiomyocyte-fibroblast interaction contributes to diabetic cardiomyopathy in mice: Role of HMGB1/TLR4/IL-33 axis.*Biochim Biophys Acta* 2015, 1852:2075-2085.
11. Beaumont J, Lopez B, Ravassa S, Hermida N, Jose GS, Gallego I, Valencia F, Gomez-Doblas JJ, de Teresa E, Diez J, Gonzalez A: MicroRNA-19b is a potential biomarker of increased myocardial collagen cross-linking in patients with aortic stenosis and heart failure.*Sci Rep* 2017, 7:40696.
12. Hristov M, Erl W, Weber PC: Endothelial progenitor cells: mobilization, differentiation, and homing.*Arterioscler Thromb Vasc Biol* 2003, 23:1185-1189.
13. Reynolds JA, Robertson AC, Bruce IN, Alexander MY: Improving cardiovascular outcomes in rheumatic diseases: therapeutic potential of circulating endothelial progenitor cells.*Pharmacol Ther* 2014, 142:231-243.
14. Kim SW, Jin HL, Kang SM, Kim S, Yoo KJ, Jang Y, Kim HO, Yoon YS: Therapeutic effects of late outgrowth endothelial progenitor cells or mesenchymal stem cells derived from human umbilical cord blood on infarct repair.*Int J Cardiol* 2016, 203:498-507.
15. Gallet R, Dawkins J, Valle J, Simsolo E, de Couto G, Middleton R, Tseliou E, Luthringer D, Kreke M, Smith RR, et al: Exosomes secreted by cardiosphere-derived cells reduce scarring, attenuate adverse remodelling, and improve function in acute and chronic porcine myocardial infarction.*Eur Heart J* 2017, 38:201-211.
16. Maring JA, Beez CM, Falk V, Seifert M, Stamm C: Myocardial Regeneration via Progenitor Cell-Derived Exosomes.*Stem Cells Int* 2017, 2017:7849851.
17. Li X, Chen C, Wei L, Li Q, Niu X, Xu Y, Wang Y, Zhao J: Exosomes derived from endothelial progenitor cells attenuate vascular repair and accelerate reendothelialization by enhancing endothelial function.*Cytotherapy* 2016, 18:253-262.
18. Silva AM, Teixeira JH, Almeida MI, Goncalves RM, Barbosa MA, Santos SG: Extracellular Vesicles: Immunomodulatory messengers in the context of tissue repair/regeneration.*Eur J Pharm Sci* 2017, 98:86-95.
19. Thery C, Zitvogel L, Amigorena S: Exosomes: composition, biogenesis and function.*Nat Rev Immunol* 2002, 2:569-579.
20. Schneider A, Simons M: Exosomes: vesicular carriers for intercellular communication in neurodegenerative disorders.*Cell Tissue Res* 2013, 352:33-47.
21. Li X, Jiang C, Zhao J: Human endothelial progenitor cells-derived exosomes accelerate cutaneous wound healing in diabetic rats by promoting endothelial function.*J Diabetes Complications* 2016, 30:986-992.
22. Wu X, Liu Z, Hu L, Gu W, Zhu L: Exosomes derived from endothelial progenitor cells ameliorate acute lung injury by transferring miR-126.*Exp Cell Res* 2018, 370:13-23.

23. Ke X, Yang D, Liang J, Wang X, Wu S, Wang X, Hu C: Human Endothelial Progenitor Cell-Derived Exosomes Increase Proliferation and Angiogenesis in Cardiac Fibroblasts by Promoting the Mesenchymal-Endothelial Transition and Reducing High Mobility Group Box 1 Protein B1 Expression.*DNA Cell Biol* 2017, 36:1018-1028.
24. Abak A, Amini S, Sakhinia E, Abhari A: MicroRNA-221: biogenesis, function and signatures in human cancers.*Eur Rev Med Pharmacol Sci* 2018, 22:3094-3117.
25. Calin GA, Croce CM: MicroRNA signatures in human cancers.*Nat Rev Cancer* 2006, 6:857-866.
26. Chen B, Li Q, Zhao B, Wang Y: Stem Cell-Derived Extracellular Vesicles as a Novel Potential Therapeutic Tool for Tissue Repair.*Stem Cells Transl Med* 2017, 6:1753-1758.
27. Cruz FF, Rocco PRM: Stem-cell extracellular vesicles and lung repair.*Stem Cell Investig* 2017, 4:78.
28. Fang L, Ellims AH, Moore XL, White DA, Taylor AJ, Chin-Dusting J, Dart AM: Circulating microRNAs as biomarkers for diffuse myocardial fibrosis in patients with hypertrophic cardiomyopathy.*J Transl Med* 2015, 13:314.
29. Tian C, Gao L, Zimmerman MC, Zucker IH: Myocardial infarction-induced microRNA-enriched exosomes contribute to cardiac Nrf2 dysregulation in chronic heart failure.*Am J Physiol Heart Circ Physiol* 2018, 314:H928-H939.
30. Yi S, Gao ZX, Zhao H, Zeng C, Luo W, Chen B, Wang WM: Identification and characterization of microRNAs involved in growth of blunt snout bream (Megalobrama amblycephala) by Solexa sequencing.*BMC Genomics* 2013, 14:754.
31. Ashburner M, Ball CA, Blake JA, Botstein D, Butler H, Cherry JM, Davis AP, Dolinski K, Dwight SS, Eppig JT, et al: Gene ontology: tool for the unification of biology. The Gene Ontology Consortium.*Nat Genet* 2000, 25:25-29.
32. Kanehisa M, Goto S, Kawashima S, Okuno Y, Hattori M: The KEGG resource for deciphering the genome.*Nucleic Acids Res* 2004, 32:D277-280.
33. Mackowiak SD: Identification of novel and known miRNAs in deep-sequencing data with miRDeep2.*Curr Protoc Bioinformatics* 2011, Chapter 12:Unit 12.10.
34. Wang J, Liu X, Lu H, Jiang C, Cui X, Yu L, Fu X, Li Q, Wang J: CXCR4(+)CD45(-) BMMNC subpopulation is superior to unfractionated BMMNCs for protection after ischemic stroke in mice.*Brain Behav Immun* 2015, 45:98-108.
35. Fan Z, Guan J: Antifibrotic therapies to control cardiac fibrosis.*Biomater Res* 2016, 20:13.
36. Goldbergova MP, Lipkova J, Fedorko J, Sevcikova J, Parenica J, Spinar J, Masarik M, Vasku A: MicroRNAs in pathophysiology of acute myocardial infarction and cardiogenic shock.*Bratisl Lek Listy* 2018, 119:341-347.
37. Sahoo S, Losordo DW: Exosomes and cardiac repair after myocardial infarction.*Circ Res* 2014, 114:333-344.
38. Henning RJ: Cardiovascular Exosomes and MicroRNAs in Cardiovascular Physiology and Pathophysiology.*J Cardiovasc Transl Res* 2020.

39. Bu D, Su Z, Meng M, Wang C: Integrative Analysis of Expression Profiles of MicroRNAs and mRNAs in Treatment of Acute Myocardial Infarction with Compound Longmaining Decoction.*Med Sci Monit* 2019, 25:9028-9041.
40. Chen Z, Li C, Lin K, Zhang Q, Chen Y, Rao L: MicroRNAs in acute myocardial infarction: Evident value as novel biomarkers?*Anatol J Cardiol* 2018, 19:140-147.
41. Morelli MB, Shu J, Sardu C, Matarese A, Santulli G: Cardiosomal microRNAs Are Essential in Post-Infarction Myofibroblast Phenoconversion.*Int J Mol Sci* 2019, 21.
42. Chen Y, Zhao Y, Chen W, Xie L, Zhao ZA, Yang J, Chen Y, Lei W, Shen Z: MicroRNA-133 overexpression promotes the therapeutic efficacy of mesenchymal stem cells on acute myocardial infarction.*Stem Cell Res Ther* 2017, 8:268.
43. Li J, Cai SX, He Q, Zhang H, Friedberg D, Wang F, Redington AN: Intravenous miR-144 reduces left ventricular remodeling after myocardial infarction.*Basic Res Cardiol* 2018, 113:36.
44. Li P, Li SY, Liu M, Ruan JW, Wang ZD, Xie WC: Value of the expression of miR-208, miR-494, miR-499 and miR-1303 in early diagnosis of acute myocardial infarction.*Life Sci* 2019, 232:116547.
45. Chen CH, Hsu SY, Chiu CC, Leu S: MicroRNA-21 Mediates the Protective Effect of Cardiomyocyte-Derived Conditioned Medium on Ameliorating Myocardial Infarction in Rats.*Cells* 2019, 8.
46. Cai S, Cheng X, Pan X, Li J: Emerging role of exosomes in liver physiology and pathology.*Hepatol Res* 2017, 47:194-203.
47. Luo Q, Guo D, Liu G, Chen G, Hang M, Jin M: Exosomes from MiR-126-overexpressing adscs are therapeutic in relieving acute myocardial ischaemic injury.*Cellular Physiology and Biochemistry* 2017, 44:2105-2116.
48. Zhu L-P, Tian T, Wang J-Y, He J-N, Chen T, Pan M, Xu L, Zhang H-x, Qiu X-T, Li C-C: Hypoxia-elicited mesenchymal stem cell-derived exosomes facilitates cardiac repair through miR-125b-mediated prevention of cell death in myocardial infarction.*Theranostics* 2018, 8:6163.
49. Ling H, Guo Z, Shi Y, Zhang L, Song C: Serum Exosomal MicroRNA-21, MicroRNA-126, and PTEN Are Novel Biomarkers for Diagnosis of Acute Coronary Syndrome.*Front Physiol* 2020, 11:654.
50. Zhu W, Yang L, Shan H, Zhang Y, Zhou R, Su Z, Du Z: MicroRNA expression analysis: clinical advantage of propranolol reveals key microRNAs in myocardial infarction.*PLoS One* 2011, 6:e14736.
51. D'Alessandra Y, Pompilio G, Capogrossi MC: MicroRNAs and myocardial infarction.*Curr Opin Cardiol* 2012, 27:228-235.
52. Vaskova E, Ikeda G, Tada Y, Wahlquist C, Mercola M, Yang PC: Sacubitril/Valsartan Improves Cardiac Function and Decreases Myocardial Fibrosis Via Downregulation of Exosomal miR-181a in a Rodent Chronic Myocardial Infarction Model.*J Am Heart Assoc* 2020, 9:e015640.
53. Arif M, Pandey R, Alam P, Jiang S, Sadayappan S, Paul A, Ahmed RPH: MicroRNA-210-mediated proliferation, survival, and angiogenesis promote cardiac repair post myocardial infarction in rodents.*J Mol Med (Berl)* 2017, 95:1369-1385.

54. Wang X, Morelli MB, Matarese A, Sardu C, Santulli G: Cardiomyocyte-derived exosomal microRNA-92a mediates post-ischemic myofibroblast activation both in vitro and ex vivo.*ESC Heart Fail* 2020, 7:284-288.
55. Fan ZG, Qu XL, Chu P, Gao YL, Gao XF, Chen SL, Tian NL: MicroRNA-210 promotes angiogenesis in acute myocardial infarction.*Mol Med Rep* 2018, 17:5658-5665.
56. Liu S, Chen J, Shi J, Zhou W, Wang L, Fang W, Zhong Y, Chen X, Chen Y, Sabri A, Liu S: M1-like macrophage-derived exosomes suppress angiogenesis and exacerbate cardiac dysfunction in a myocardial infarction microenvironment.*Basic Res Cardiol* 2020, 115:22.
57. Ma T, Chen Y, Chen Y, Meng Q, Sun J, Shao L, Yu Y, Huang H, Hu Y, Yang Z, et al: MicroRNA-132, Delivered by Mesenchymal Stem Cell-Derived Exosomes, Promote Angiogenesis in Myocardial Infarction.*Stem Cells Int* 2018, 2018:3290372.
58. Bayoumi AS, Teoh JP, Aonuma T, Yuan Z, Ruan X, Tang Y, Su H, Weintraub NL, Kim IM: MicroRNA-532 protects the heart in acute myocardial infarction, and represses prss23, a positive regulator of endothelial-to-mesenchymal transition.*Cardiovasc Res* 2017, 113:1603-1614.
59. Yuan J, Chen H, Ge D, Xu Y, Xu H, Yang Y, Gu M, Zhou Y, Zhu J, Ge T, et al: Mir-21 Promotes Cardiac Fibrosis After Myocardial Infarction Via Targeting Smad7.*Cell Physiol Biochem* 2017, 42:2207-2219.
60. Bayoumi AS, Park KM, Wang Y, Teoh JP, Aonuma T, Tang Y, Su H, Weintraub NL, Kim IM: A carvedilol-responsive microRNA, miR-125b-5p protects the heart from acute myocardial infarction by repressing pro-apoptotic bak1 and klf13 in cardiomyocytes.*J Mol Cell Cardiol* 2018, 114:72-82.
61. Dai Y, Wang S, Chang S, Ren D, Shali S, Li C, Yang H, Huang Z, Ge J: M2 macrophage-derived exosomes carry microRNA-148a to alleviate myocardial ischemia/reperfusion injury via inhibiting TXNIP and the TLR4/NF-kappaB/NLRP3 inflammasome signaling pathway.*J Mol Cell Cardiol* 2020, 142:65-79.
62. Li W, Wang Q, Feng Q, Wang F, Yan Q, Gao SJ, Lu C: Oncogenic KSHV-encoded interferon regulatory factor upregulates HMGB2 and CMPK1 expression to promote cell invasion by disrupting a complex lncRNA-OIP5-AS1/miR-218-5p network.*PLoS Pathog* 2019, 15:e1007578.
63. Satapathy SR, Nayak A, Siddharth S, Das S, Nayak D, Kundu CN: Metallic gold and bioactive quinacrine hybrid nanoparticles inhibit oral cancer stem cell and angiogenesis by deregulating inflammatory cytokines in p53 dependent manner.*Nanomedicine* 2018, 14:883-896.
64. Li P, Lv X, Zhang Z, Xie S: S100A6/miR193a regulates the proliferation, invasion, migration and angiogenesis of lung cancer cells through the P53 acetylation.*Am J Transl Res* 2019, 11:4634-4649.
65. Florence ME, Massuda JY, Soares TC, Stelini RF, Poppe LM, Brocker EB, Metze K, Cintra ML, de Souza EM: p53 immunoexpression in stepwise progression of cutaneous squamous cell carcinoma and correlation with angiogenesis and cellular proliferation.*Pathol Res Pract* 2015, 211:782-788.
66. Ubil E, Duan J, Pillai IC, Rosa-Garrido M, Wu Y, Bargiacchi F, Lu Y, Stanbouly S, Huang J, Rojas M, et al: Mesenchymal-endothelial transition contributes to cardiac neovascularization.*Nature* 2014, 514:585-590.
67. Adighibe O, Pezzella F: The Role of JMY in p53 Regulation.*Cancers (Basel)* 2018, 10.

Figures

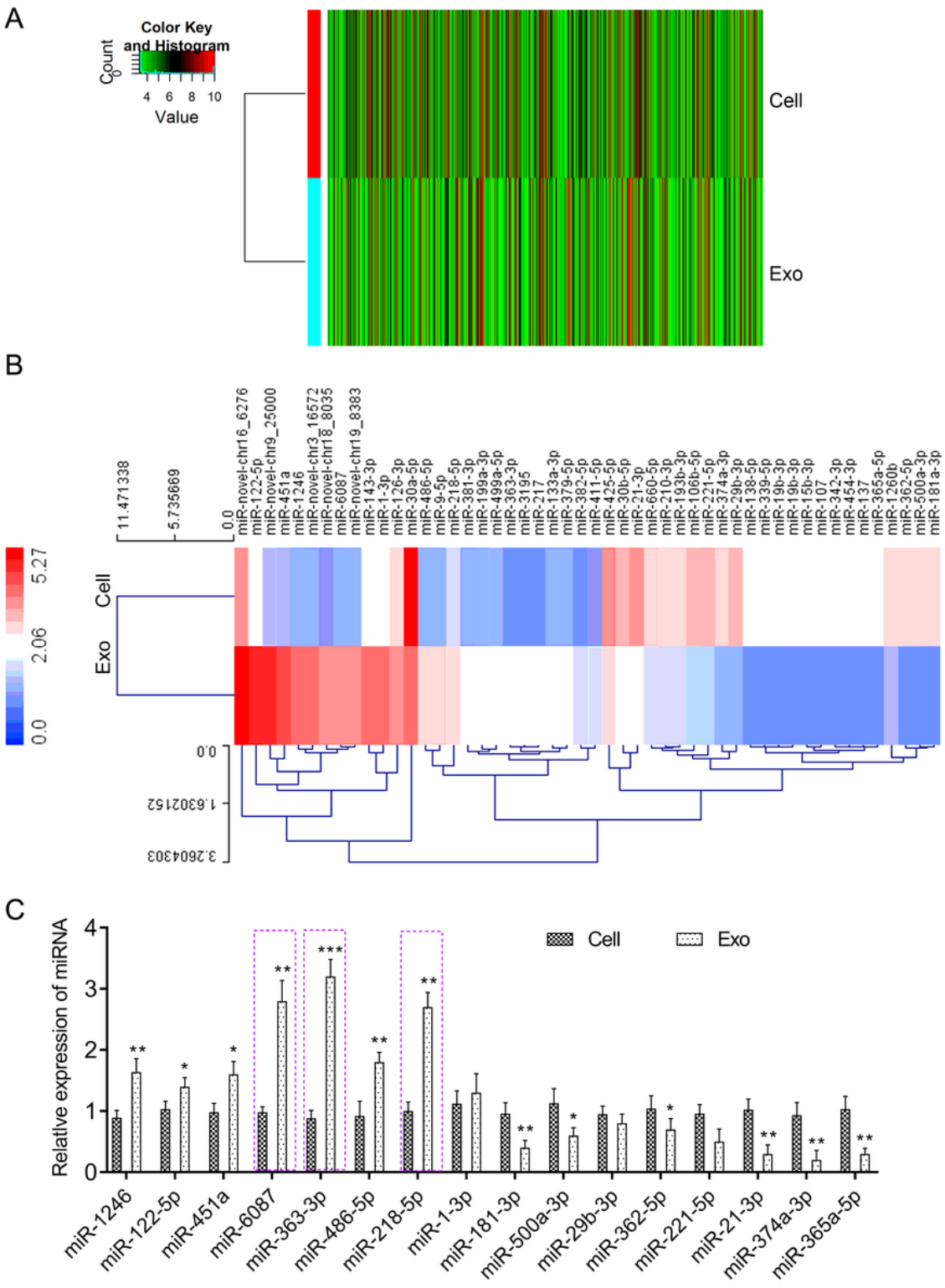

Figure 1

Differential miRNA expression profiles between EPCs and EPC-Exos. A). Hierarchical clustering of differentially expressed miRNAs between EPCs and EPC-Exos, which are displayed on a scale from green (low) to red (high). B). Hierarchical clustering heat map of the clearly distinct differentially expressed

miRNAs in EPCs and EPC-Exos, ranging from red (relatively high miRNA expression) to blue (relatively low miRNA expression). The miRNAs in the heat map are clustered based on the relative expression patterns. C). The relative expression levels of sixteen differentially expressed miRNAs (eight upregulated and eight downregulated) in EPC-Exos compared with EPCs were measured with qRT-PCR. The data are presented as the mean ± SD (n = 3). *P < 0.05, **P < 0.01, ***P < 0.001 EPC-Exos versus EPCs.

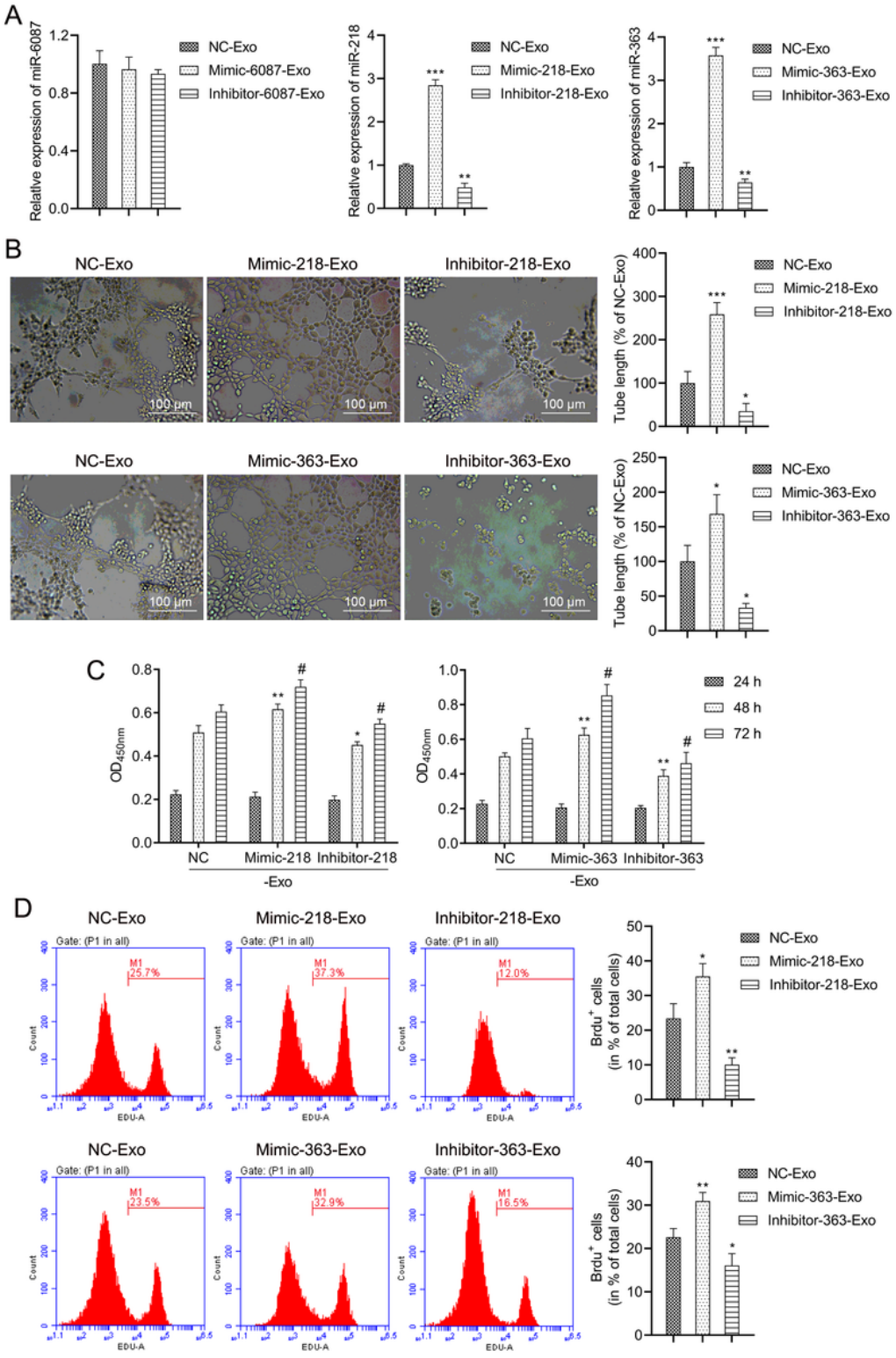

Figure 2

miR-218-5p and miR-363-3p promoted angiogenesis and proliferation of CFs. A). The relative expression levels of miR-6087, miR-218-5p and miR-363-3p mimics and inhibitors were measured with qRT-PCR. The data are presented as the mean ± SD (n = 3). **P < 0.01, ***P < 0.001 mimic-Exo or inhibitor-Exo versus NC-Exo. B). Tube formation capability and relative tube length were increased in the miR-218-5p and miR-363-3p mimic-Exo groups and decreased in inhibitor-Exo groups. The data are presented as the mean ± SD (n = 3). *P < 0.05, ***P < 0.001 mimic-Exo or inhibitor-Exo versus NC-Exo. C). CCK8 assay to detect the effect of exosomal miR-218-5p and miR-363-3p on cell proliferation. The data are presented as the mean ± SD (n = 3). * # P < 0.05, **P < 0.01, mimic-Exo or inhibitor-Exo versus NC-Exo. D). BrdU labelling and flow cytometry assay to detect the effect of exosomal miR-218-5p and miR-363-3p on cell proliferation. The data are presented as the mean ± SD (n = 3). *P < 0.05, **P < 0.01, mimic-Exo or inhibitor-Exo versus NC-Exo.

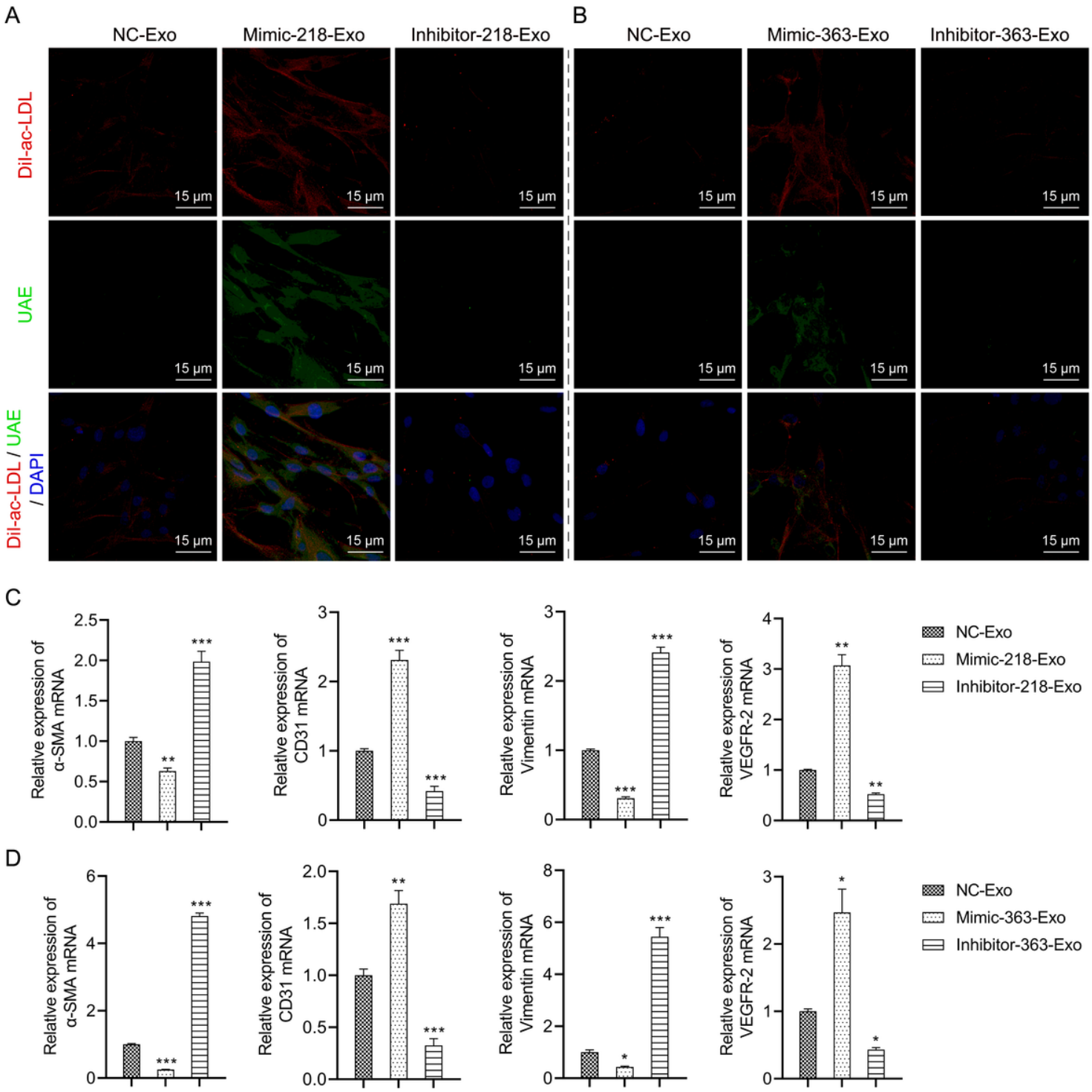

Figure 3

miR-218-5p and miR-363-3p promoted mesenchymal-endothelial transition in CFs. A). A phagocytosis assay was performed to detect the engulfment of DiI-Ac-LDL and binding to endothelial-specific lectin FITC-UEA-1 by CFs treated with mimic-218-Exo or inhibitor-218-Exo. Magnification: 120×. B). A phagocytosis assay was performed to detect the engulfment of DiI-Ac-LDL and binding to endothelial-specific lectin FITC-UEA-1 by CFs treated with mimic-363-Exo or inhibitor-363-Exo. Magnification: 120×. C). qRT-PCR detection of the relative expression levels of CD31, VEGFR-2, α-SMA and vimentin in CFs

treated with mimic-218-Exo or inhibitor-218-Exo. The data are presented as the mean ± SD (n = 3). **P < 0.01, ***P < 0.001, mimic-Exo or inhibitor-Exo versus NC-Exo. D). qRT-PCR detection of the relative expression levels of CD31, VEGFR-2, α-SMA and vimentin in CFs treated with mimic-363-Exo or inhibitor-363-Exo. The data are presented as the mean ± SD (n = 3). *P < 0.05, **P < 0.01, ***P < 0.001 mimic-Exo or inhibitor-Exo versus NC-Exo.

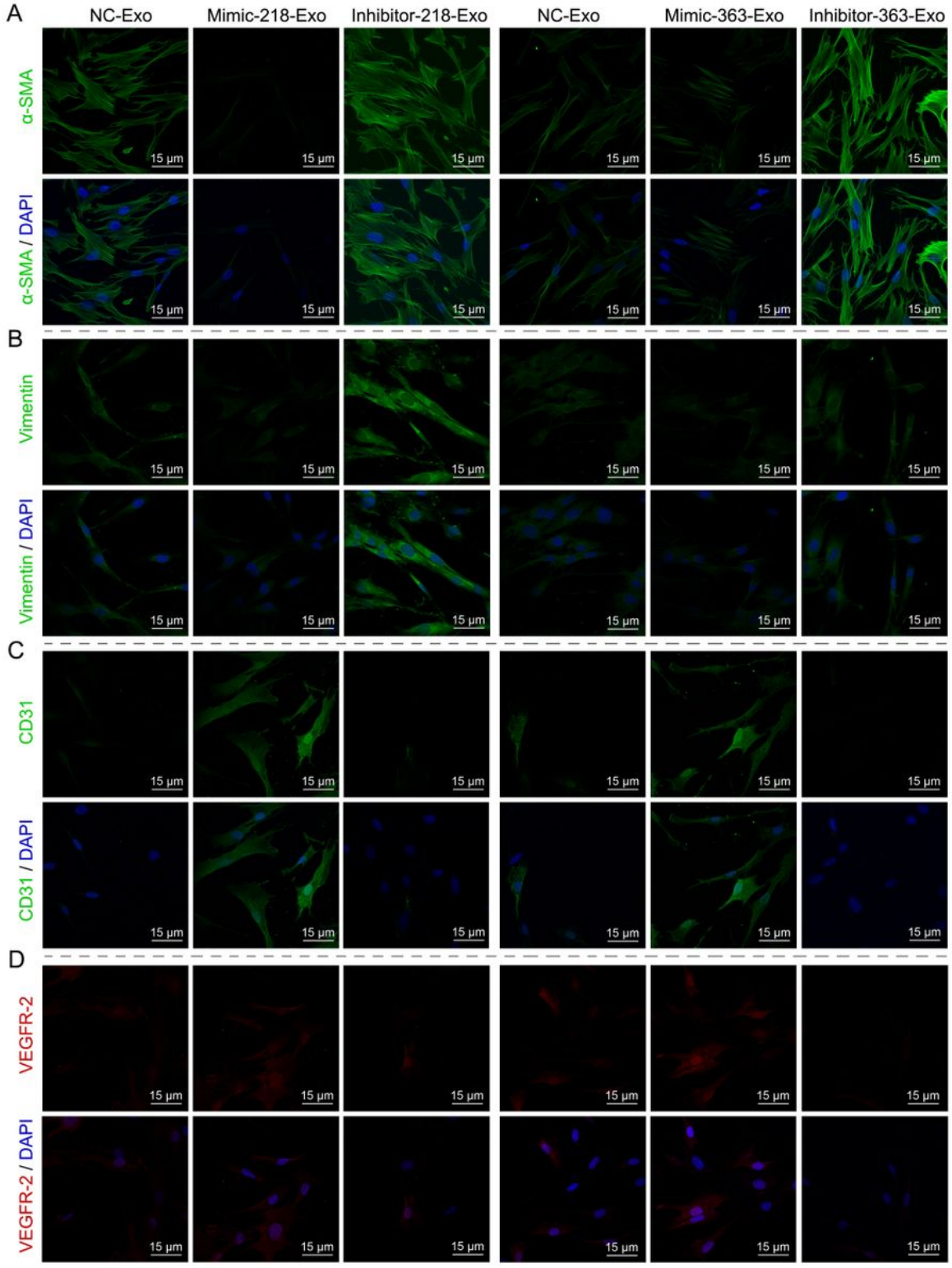

Figure 4

Immunofluorescence staining to detect the relative expression levels of α-SMA (A), vimentin (B), CD31 (C) and VEGFR-2 (D) in CFs treated with miR-218-5p and miR-363-3p mimics and inhibitors. The photographs were taken with a laser confocal microscope (Zeiss, LSM700), Magnification: 120×.

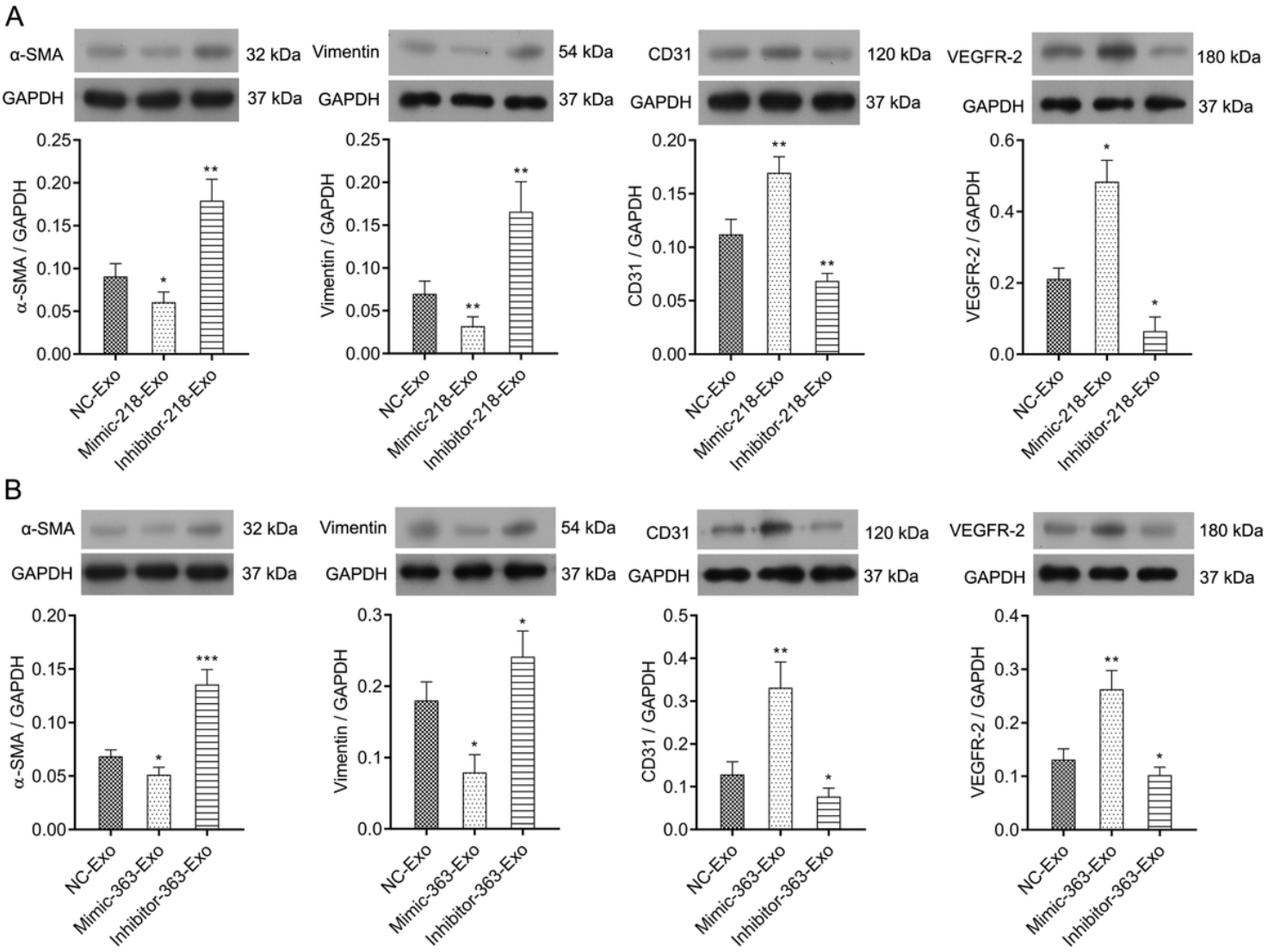

Figure 5

Western blot analysis to detect the relative expression levels of CD31, VEGFR-2, α-SMA and vimentin in CFs treated with miR-218-5p (A) and miR-363-3p (B) mimic-Exo and inhibitor-Exo. The data are presented as the mean ± SD (n = 3). *P < 0.05, **P < 0.01, ***P < 0.001 mimic-Exo or inhibitor-Exo versus NC-Exo.

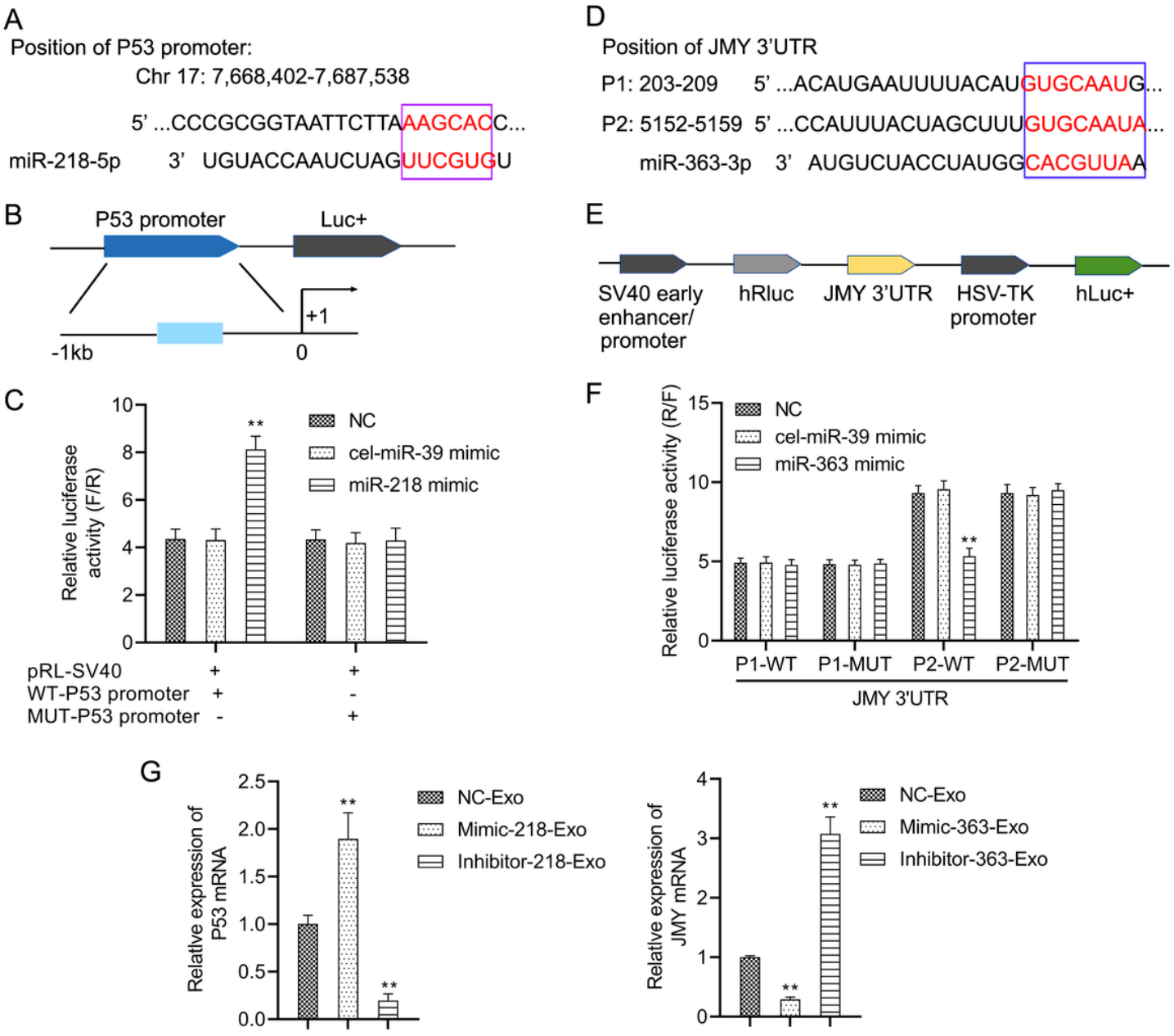

Figure 6

P53/JMY as a target of miR-218-5p and miR-363-3p. A). The predicted binding sites for miR-218-5p in the P53 promoter. B). Schematic diagram of pGL3 Basic vector construction harboring P53 promoter binding sites. C). Relative luciferase activity (F/R) assay for miR-218-5p binding to the P53 promoter. Cel-miR-39 mimic served as the negative control. The data are presented as the mean ± SD (n = 3), **P < 0.01 miR-218-5p mimic versus NC or cel-miR-39 mimic. D). The predicted binding sites for miR-363-3p in the 3'UTR of JMY. E). Schematic diagram of psi-Check2 vector construct harboring the 3'UTR of JMY binding sites. F). Relative luciferase activity (R/F) assay for miR-363-3p in the 3'UTR of JMY. The data are presented as the mean ± SD (n = 3), **P < 0.01 miR-363-3p mimic versus NC or cel-miR-39 mimic. Cel-miR-39 mimic served as the negative control. G). qRT-PCR to detect the relative expression levels of P53 and JMY in CFs

in the mimic-Exo and inhibitor-Exo groups. The data are presented as the mean ± SD (n = 3). *P < 0.05, **P < 0.01 mimic-Exo or inhibitor-Exo versus NC-Exo.

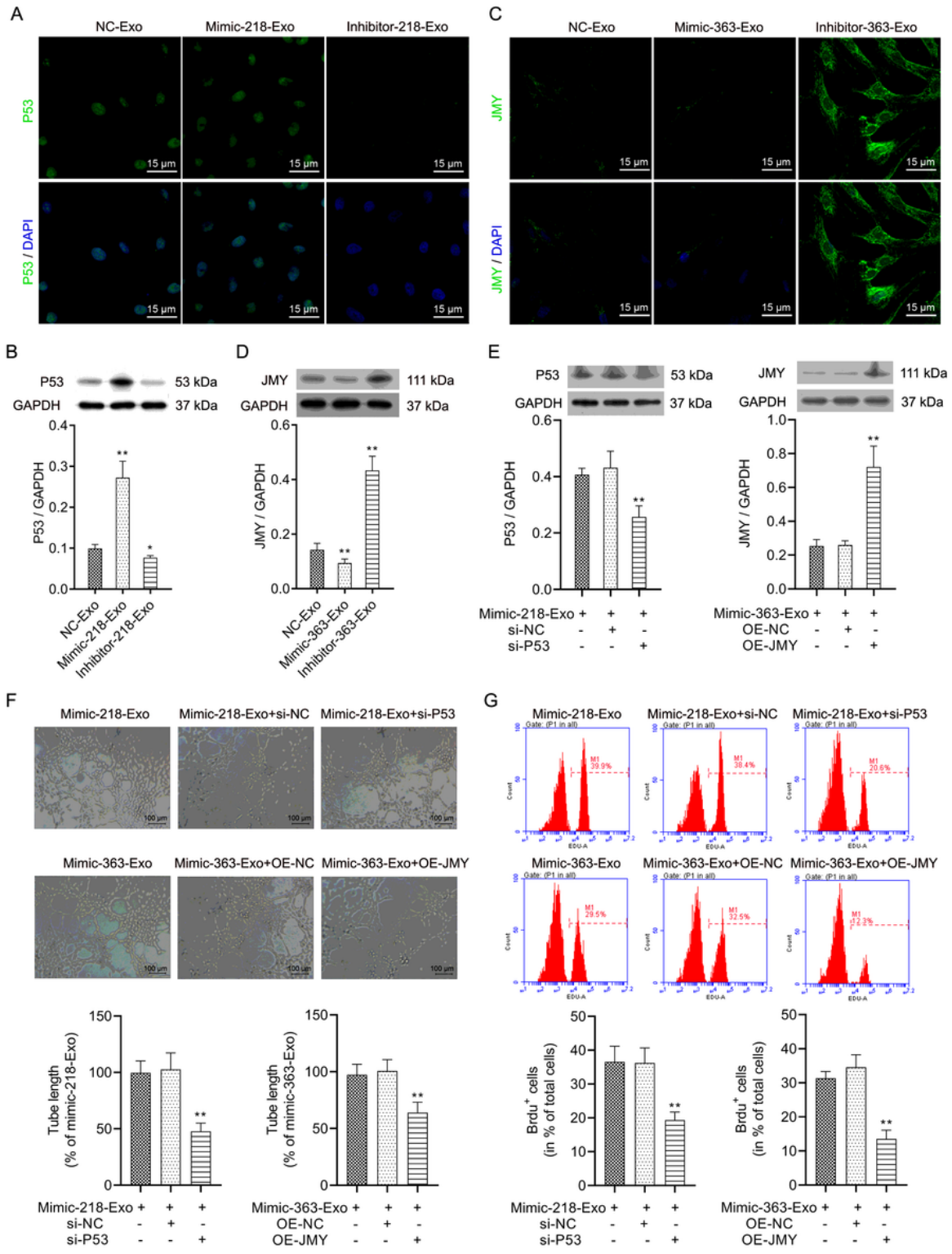

Figure 7

Effect of miR-218-5p and miR-363-3p on P53/JMY. A and C). Immunofluorescence staining for the relative expression levels of P53 and JMY in CFs, in the miR-218-5p/miR-363-3p mimic-Exo and inhibitor-Exo groups. B and D). Western blot analysis to detect the relative expression levels of P53 and JMY in

miR-218-5p/miR-363-3p mimic-Exo and inhibitor-Exo groups in CFs, respectively. The photographs were taken with a laser confocal microscope (Zeiss, LSM700), Magnification: 120×. The data are presented as the mean ± SD (n = 3). *P < 0.05, **P < 0.01 mimic-Exo or inhibitor-Exo versus NC-Exo. E). Western blot analysis to detect the relative expression levels of P53 and JMY in si-P53 and OE-JMY CF groups, respectively. The data are presented as the mean ± SD (n = 3). **P < 0.01, si-P53 or OE-JMY group versus Mimic-218-Exo or Mimic-363-Exo group. F). The tube formation capability and relative tube length were decreased in the si-P53 and OE-JMY groups. The data are presented as the mean ± SD (n = 3). **P < 0.01, si-P53 or OE-JMY group versus Mimic-218-Exo or Mimic-363-Exo group. G). BrdU labelling and flow cytometry assay to detect the effect of si-P53 and OE-JMY on cell proliferation. The data are presented as the mean ± SD (n = 3). **P < 0.01, si-P53 or OE-JMY group versus Mimic-218-Exo or Mimic-363-Exo group.

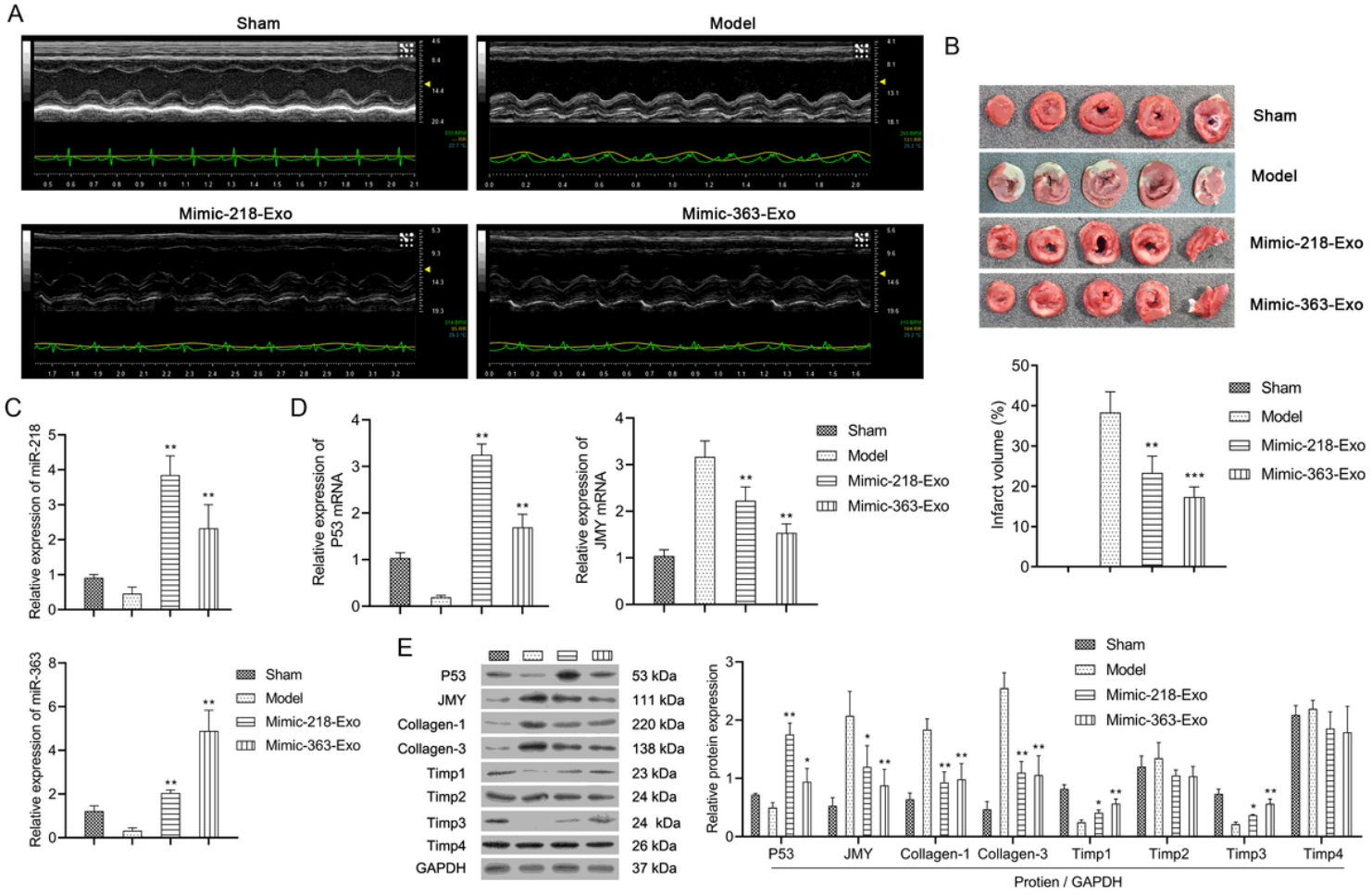

Figure 8

Effect of exosomal miR-218-5p and miR-363-3p on cardiac features and function in MI rats. A). A representative ECG of LCA-induced MI rats in the different groups (Sham, Model, miR-218-5p and miR-363-3p mimic-Exo). B). TTC staining of heart tissues from the Sham, Model, and mimic-Exo groups. The data are presented as the mean ± SD (n = 10). **P < 0.01, ***P < 0.001 mimic-Exo versus model. C-D). qRT-PCR to detect the relative expression levels of miR-218-5p, miR-363-3p, P53 and JMY in the mimic-

Exo groups. E). The protein expression of P53, JMY, Collagen-1/3 and Timp1-4 in the different groups. The data are presented as the mean ± SD (n = 10). *P < 0.05, **P < 0.01 mimic-Exo versus model.

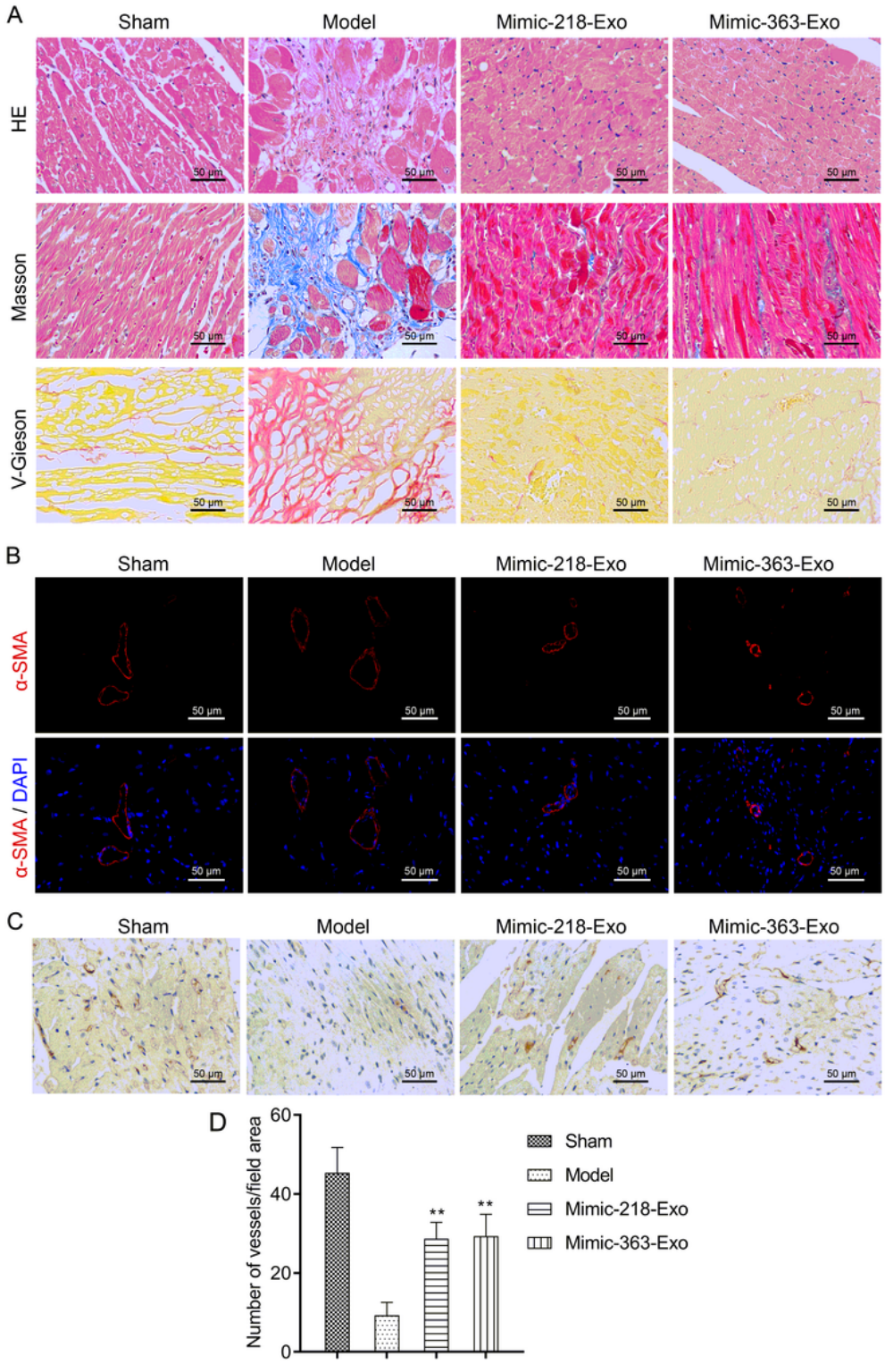

Figure 9

Exosomal miR-218-5p and miR-363-3p alleviate LCA-induced myocardial infarction. A). H&E, Masson and Van Gieson staining of heart tissues treated with EPC-Exos containing miR-218-5p mimic or miR-363-3p mimic. Magnification: 40×. B). Immunofluorescence staining for the relative expression levels of α-SMA in

heart tissues treated with EPC-Exos containing miR-218-5p mimic or miR-363-3p mimic. Magnification: 40×. C). Immunohistochemistry for vWF in heart tissues treated with EPC-Exos containing miR-218-5p mimic or miR-363-3p mimic. D). The number of vessels/field area in the remodeled left ventricle. The data are presented as the mean ± SD (n = 3). **P < 0.01 mimic versus model.

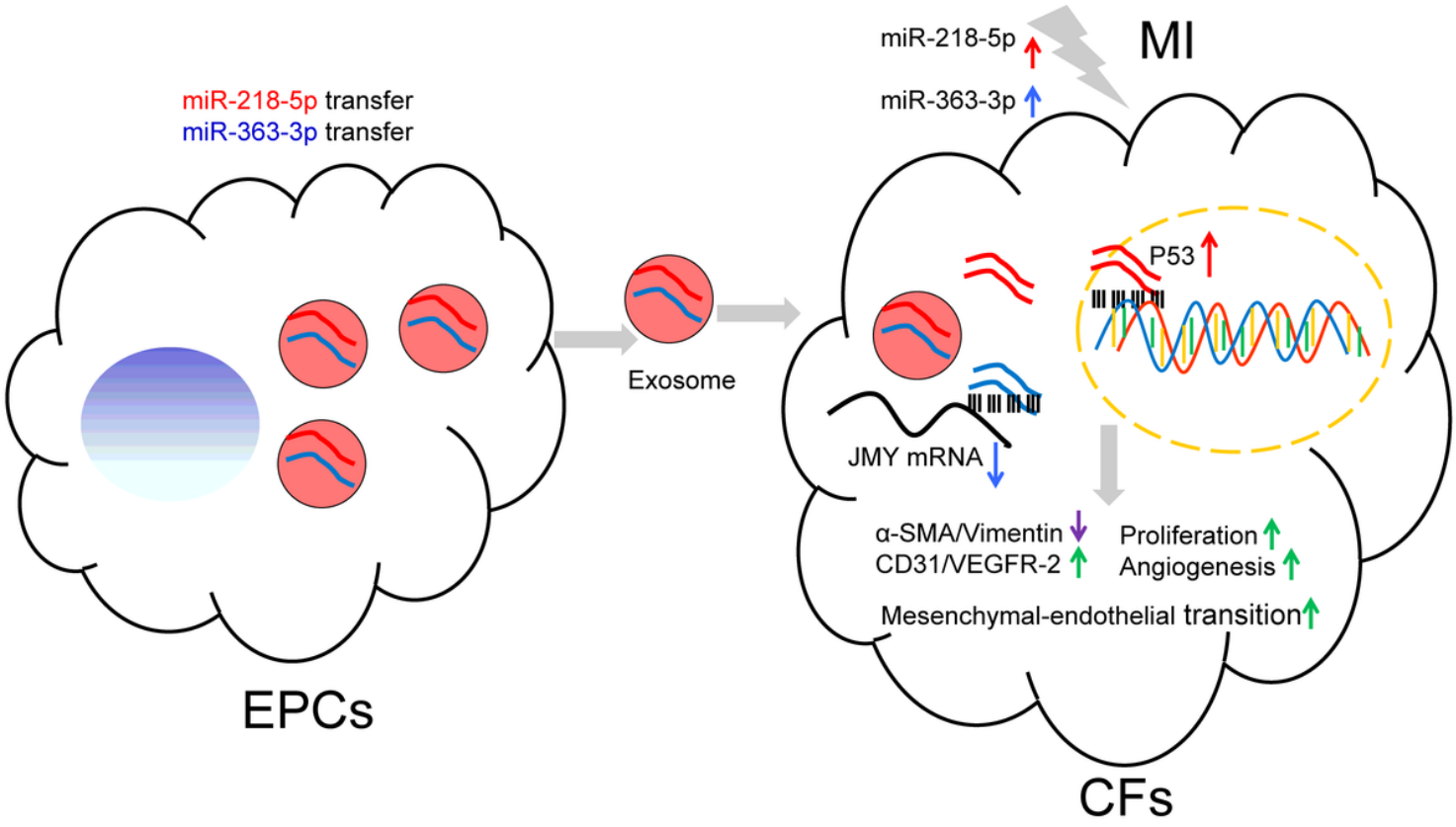

Figure 10

Model of the molecular mechanism of exosomal miR-218-5p/miR-363-3p in myocardial infarction. Exosomal miR-218-5p and miR-363-3p from endothelial progenitor cells can target the P53 promoter and 3' UTR of JMY, respectively. The increased/decreased expression of P53/JMY promotes angiogenesis, proliferation and mesenchymal-endothelial transition of CFs by downregulating α-SMA and vimentin and upregulating CD31 and VEGFR-2, which further alleviate LCA-induced chronic myocardial infarction.

Supplementary Files

This is a list of supplementary files associated with this preprint. Click to download.

- SupplementalFigure1.tif
- SupplementalFigure2.tif
- SupplementalFigure3.tif
- SupplementalFigure4.tif
- Supplementalfigure5.tif

- SupplementalFigure6.tif
- SupplementalTable1.docx
- SupplementalTable2.docx